12-13-2021

Effects of video game playing on sensorimotor decision-making abilities and brain network dynamics

Timothy Jordan

Effects of video game playing on sensorimotor decision-making abilities and brain network dynamics

by

Timothy Jason Jordan

Under the Direction of Mukesh Dhamala, PhD

ABSTRACT

Video game playing is a popular activity that provides a cognitively engaging, sensory rich, competitive environment. Sensorimotor decision-making is a dynamic brain process involving multiple steps that build to make and execute a choice. This dissertation examines the differences in brain mechanisms for decision-making between those who play video games extensively and those who do not for two studies. These studies of video gamers and non-gamers investigated the differences between commonly activated brain regions from both groups and the differences in brain network interactions. We used a modified moving dot left-right discrimination task to examine each group's decision-making performance and functional magnetic resonance imaging (fMRI) to record the underlying brain activity asso-

ciated with task completion. Participants had to make decisions about the direction (left or right) of motion of a specific set of color dots. Video game players (VGP) were found to be faster than non-video game players (NVGP) by approximately 190 milliseconds and overall approximately 2% more accurate. In the commonly activated regions study, we extracted the percent signal change above baseline due to task-induced activity. VGP showed higher levels of percent signal change than NVGP for primary and secondary visual areas and premotor and motor regions. Functional Connectivity (FC) analysis allowed us to examine if the activity from one correlates with the other. Examining FC for commonly activated regions, we found six undirected and four directed increased connections across those regions. We found that VGP displayed increased connections from DLPFC. These findings suggest that VGP perform better on decision-making tasks because of enhanced attention control and visuomotor coordination. For between network interactions, we examined previously studied decision-making related networks, CEN-SN-DMN, and attention switching networks, DAN-DMN-SN. VGP displayed decreased connectivity from SN to DAN, DMN, and CEN but showed increased connectivity to SN. These findings imply that VGP increases their performance by controlling the SN instead of SN controlling network interactions. These results provide an improved understanding of how cognitively engaging tasks, like video game playing, enhance our abilities to perform sensorimotor tasks even outside of video game playing.

INDEX WORDS: Perceptual Decision-Making, Functional Magnetic Resonance Imaging (fMRI), Granger Causality (GC), Functional Connectivity (FC), Salience Network (SN), Central Executive Network (CEN), Default Mode Network (DMN), Dorsal Attention Network (DAN), Video Games, Decision Response Time

Effects of video game playing on sensorimotor decision-making abilities and brain network dynamics

by

Timothy Jason Jordan

A Dissertation Submitted in Partial Fulfillment of the Requirements for the Degree of

Doctor of Philosophy

in the College of Arts and Sciences

Georgia State University

2021

Effects of video game playing on sensorimotor decision-making abilities and brain network dynamics

by

Timothy Jason Jordan

Committee Chair:	Mukesh Dhamala
Committee:	Brian Thoms
	Sidong Lei

Electronic Version Approved:

Office of Graduate Studies

College of Arts and Sciences

Georgia State University

December 2021

DEDICATION

I'd like to dedicate this to my parents, Cathy and Michael Jordan, for all their support.

ACKNOWLEDGMENTS

Getting this far took a lot of support and help and I don't think I'll ever be able to thank all those who helped me complete this program. Firstly, I would like to thank my advisor, Dr. Mukesh Dhamala, who saw the potential in me and gave me the opportunity to come here and pursue my dream. He always supported my research and always lent his experience to my efforts. This thesis would literally not have been possible without him guiding me. I am also very grateful for my dissertation committee and the time they have given me.

I would also like to thank all those who directly aided me in my research. A major thank you to Zane Blalock and Madison Hanberry, without you both I could never have made such a complex stimulus for my study and would have had to go with a much simpler design. I'd also like to show my appreciation for Dr. Vish Ahluwalia for all your aid in not only designing my scan sequence, but all the time you gave me to show me how to do different analyses with my data. I'd like to thank my lab mates of the Neurophysics Research Group, Kiran, Sushma and Bhim, who supported me both technically and mentally throughout my entire time. And lastly, I'd like to thank Brendan Cross for helping me get through the first couple years of courses and being my study partner for our qualifier exams.

Outside of the academic environment, I'd like to thank my parents for their support throughout my entire college career and helping get this far. Special thanks to my girlfriend, Hilda, for standing by me these past years helping me through everything and helping me push forward when it was hardest. I'd like to thank all my friends for helping me along this journey in so many ways I could never had made it this far without such a good support

system. Finally, I'd like to thank all the participants in my study, not only did many of them participate and allow me to do my study, but they actively spread the word to help me get more participants.

TABLE OF CONTENTS

LIST OF TABLES

LIST OF FIGURES

LIST OF ABBREVIATIONS

dACC	dorsal Anterior Cingulate Cortex
AFNI	Analysis of Functional NeuroImages
AG	Angular Gyrus
aI	anterior Insula
BOLD	Blood-Oxygen-Level Dependent
BR	Battle Royale
CAL	Calcarine
CEN	Central Executive Network
CGC	Conditonal Granger Causality
DAN	Dorsal Attention Network
DICOM	Digital Imaging and Communications in Medicine
DLPFC	Dorsolateral Prefrontal Cortex
DMN	Default Mode Network
E0	Easy Difficulty Speed setting 0
E1	Easy Difficulty Speed setting 1

E23	Easy Difficulty Speed setting 2-3
E4	Easy Difficulty Speed setting 4
FC	Functional Connectivity
FEF	Frontal Eye Field
fMRI	Functional Magnetic Resonance Imaging
FPS	First Person Shooter
FSL	FMRIB Software Library
FWE	Family-wise error
GC	Granger Causality
GLM	General Linear Model
GMV	Gray Matter Volume
H0	Hard Difficulty Speed setting 0
H1	Hard Difficulty Speed setting 1
H2	Hard Difficulty Speed setting 2-3
H4	Hard Difficulty Speed setting 4
HPC	Hippocampus

I	Insula
IFG	Inferior Frontal Gyrus
IFO	Inferior Frontal pars orbitalis
IFT	Inferior Frontal pars triangularis
IPL	Inferior Parietal Lobe
IPS	IntraParietal Sulcus
LING	Lingual Gyrus
M0	Medium Difficulty Speed setting 0
M1	Medium Difficulty Speed setting 1
M2	Medium Difficulty Speed setting 2-3
M4	Medium Difficulty Speed setting 4
MarsBaR	MARSeille Boîte À Région d'Intérêt
MB	Midbrain
MCC	Middle Cingulate Cortex
MD	Moving Dots
MNI	Montreal Neurological Institute

MOBA	Multiplayer Online Battle Arena
MOG	Middle Occipital Gyrus
aMPFC	anterior Medial Prefrontal Cortex
ms	Milliseconds
NIFTI	Neuroimaging Informatics Technology Initiative
NVGP	Non-Video Game Player
PCC	Posterior Cingulate Cortex
PFC	Prefrontal Cortex
PoCG	PostCentral Gyrus
PPC	Posterior Parietal Cortex
PreCG	Precentral Gyrus
PUT	Putamen
ROI	Region of Interest
RTS	Real-Time Strategy
SMA	Supplementary Motor Area
SMG	SupraMarginal Gyrus

SN	Salience Network
SOG	Superior Occipital Gyrus
SPM	Statistical Parametric Mapping
TE	Echo Time
THA	Thalamus
TI	Inversion Time
TR	Repetition Time
VBM	Voxel-based Morphometry
Ver9	Vermis 9
VGP	Video Game Player
VMPFC	Ventromedial Prefrontal Cortex

CHAPTER 1
INTRODUCTION

1.1 Research Overview

Training our brains to enhance cognitive skills is a common desire in today's society. This opens the questions about the topic of how to cognitively train for specific increased capabilities. What activity provides the proper environment for training for significant increases in skills? How does it affect the brain to achieve increased cognitive abilities? This knowledge is important for understanding whether specific activities could benefit a population of untrained individuals.

Video games have evolved significantly since their public debut in the early 1970s. Far from the simplicity of the earliest video games, video games today are much more complex in the environment that players are immersed in and in the tasks demanded of them to progress or achieve victory. These graphically rich virtual environments and fast-paced challenges demand players to be quick and accurate in order to complete their goals adequately.

Players are required to discern targets from small objects off in the distance and with mass amounts of interference complicating their visual fields. Like athletic competitions, the difference between winning and losing could be a fraction of a second or a fraction of a degree of contact. Similarly, video game players (VGP) train to react more quickly and more accurately so that they do not miss their target and lose. However, unlike athletic sports, these contests are not physically demanding. Instead, they rely much more heavily on cognitive capabilities. The press of a key does not take much physical strength, but the

timing and speed of the press take a trained amount of cognitive specificity to achieve the player's goal. These types of environments have within them the potential to alter cognitive functions by their innate requirements.

Within the span of one game, players must make hundreds of choices in the moment, weighing the pros and cons of each choice and how the answer will help them achieve victory. The sensorimotor decision-making process itself is highly complex, involving the integration of information across multiple sub-processes including sensation, perception, and action (Siegel et al. (2011), Siegel et al. (2015)). To make the correct choice, information must be sorted and filtered correctly so that only relevant rich information influences the outcome. The complexity and allowed time of a decision can make it difficult for a person to arrive at the correct answer. Thus, the desire to increase our ability to make quick decisions while maintaining accuracy pushes us to find ways of training our decision-making skills.

The study of a cognitive benefit from playing video games is of great debate. While people see the potential video games possess in training cognitive skills, precise results demonstrating that underlying neural mechanisms correlate with these changes have yet to be shown. This dissertation examines the brain activity and connectivity due to video game playing by studying the roles of specified regions to come together as a network in decision-making tasks. This study is important not only to provide a potential method of training cognitive skills oriented to decision making but also to illuminate the underlying neural mechanisms that are changed by this type of training.

Brain imaging techniques, such as functional MRI, offer a way to study exactly where cognitive activities are being carried out in the brain, such as decision-making, utilizing the

Blood-Oxygen Level Dependent (BOLD) signal measurement. The BOLD signal measures the amount of deoxygenated blood present in the blood vessels in the brain, which indirectly correlates to brain activity (Glover (2011)). For this study, we used functional Magnetic Resonance Imaging (MRI) to record these brain activities as participants completed decision-making tasks to see how the video game player brain works. In the chapters that follow, I discuss the behavior and brain differences for decision-making between those who play video games and those who do not, especially **(i)** how video game playing changes decision time and **(ii)** modulates network interactions for decision making, and **(iii)** how video game playing alters attention control networks for task-focused activities.

1.2 Background & Significance

Since their public release in the 1970s, the effect of video games on a person has been debated, with many people early on and some today believing that they cause negative effects. These perceived effects range from shortening attention spans to increasing violent behaviors. Even today, where we have professional gaming leagues, public perception is mixed on the topic, and the science is still building to change that perception. Over the past two decades, research projects have tried to study the effects of video games on behavior and cognitive skills to see what differences there may be between gaming and non-gaming populations.

The majority of the studies on video games have been task performance assessments that implicate certain cognitive functions. These studies showed that VGP have multiple benefits for cognitive skills when compared to non-video game players (NVGP). VGPs showed

increased working memory (Anguera et al. (2013), Basak et al. (2008)), better attention control (Anguera et al. (2013), Green & Bavelier (2007), Green & Bavelier (2015), Wu & Spence (2013)), greater spatial resolution (Green & Bavelier (2007), Li et al. (2009)), more efficient task switching (Basak et al. (2008), Oei & Patterson (2014)), and improved decision making (Reynaldo et al. (2021)). These results were not exclusive to those who had played for years, but also seen in those trained for a certain number of hours in a time span (Anguera et al. (2013), Lynch et al. (2010), Rosser (2007), Wu & Spence (2013)).

While these studies give insight into the large-scale cognitive benefits of video games, the neural underpinnings of the benefits have yet to be determined. Brain imaging studies on VGP are much more limited in what they have examined. Around half the studies have looked solely at how video game playing correlates to violence, and the other half have primarily been resting-state studies of VGP in video game environments via presented pictures or are examining addictive effects of gaming (Palaus et al. (2017)). These studies have primary looked at brain activations (Granek et al. (2010), Richlan et al. (2017)), resting-state functional connectivity (Momi et al. (2020)) and voxel-based morphometry (Tanaka et al. (2013)). These studies examine neural differences between VGP and NVGP, but they still leave out the active task performance neural connections involved. Thus, this study aimed to examine how the task-focused neural activations and connections differed for VGP and NVGP.

In this study, we wanted to examine different ways video games affected brain mechanisms controlling cognitive skills. We chose for our study to image participants while they completed a decision-making behavioral task to engage previously studied cognitive skills

as stated above. We aimed first to show performance differences similar to previous studies and then examine those behavior differences from the perspective of neural mechanism differences. Specifically, we want to examine these five questions:

1. What regional activity differences are present between VGP and NVGP for decision-making tasks?

2. How are region to region functional connections, non-directional and directional, different for VGP?

3. What are the brain structural differences between VGP and NVGP?

4. How does video game playing change network interactions for decision-making?

5. How does video game playing change network interactions switching from resting state to task-active state?

1.3 Hypotheses

For this study, we hypothesized that:

1. VGP would display improved task performance, both accuracy and response time

2. VGP will display elevated activations and connectivity between visuomotor regions. This is based on previous research showing increased attention control and visual processing (Green & Bavelier (2003), Green & Bavelier (2007), Wu & Spence (2013)).

3. VGP will increased grey matter volume in task-related regions similar to findings in previous studies (Han et al. (2012), Tanaka et al. (2013)).

4. VGP will show increased connectivity and control from the Salience Network (SN) in consistency with previous findings that (i) SN drives rest to task switching and decision-making performance (Chand & Dhamala (2016), Zhou et al. (2017)) and (ii) resting state network activity between SN and CEN is increased for VGP (Gong et al. (2016)).

1.4 Structure of Dissertation

Chapter 2 has a description of study materials, methods, and analyses used. Chapter 3 contains the results for the task-related behavioral response, brain node, and network activities. Chapter 3 Section 4 is divided into three subsections to show the results from the task-related regional activity, decision-making networks, and attention switching network. Chapter 4 Section 1 is divided into subsections task-related regional activity, decision-making networks, and attention switching networks to discuss the findings of each result. This dissertation is based on the following two articles:

- T. Jordan and M. Dhamala, "Effects of video game playing on sensorimotor decision-making abilities and brain network dynamics". (In Preparation for Submission)

- T. Jordan and M. Dhamala, "Video game playing modulates salience network connectivity to improve sensorimotor decision-making task performance". (In Preparation for Submission)

CHAPTER 2
MATERIALS & METHODS

2.1 Materials

2.1.1 Participants

In this neuroimaging study, 47 people in total (28 VGP and 19 NVGP) participated. Table 2.1 shows the demographics of the participants. Each participant filled out a questionnaire about their video game playing to determine which group a person would be placed in. Participants who indicated playing over 5 hours per week in one of four types of video game genres for the last two years were considered to be video game players. The four types of VGPs we recruited were those playing one of the following: First Person Shooter (FPS), Real-Time Strategy (RTS), Multiplayer Online Battle Arena (MOBA), and Battle Royale (BR). NVGP were on average less than 30 minutes of playtime per week. All participants were required to pass the full Ishihara's Test for Color Deficiency. Participants provided signed written consent forms and health screenings prior to their scheduled scan session. Participants were compensated for their participation in the experiment. The Institutional Review Boards of Georgia State University and Georgia Institute of Technology, Atlanta, Georgia, approved this study.

Table 2.1 Participant Demographics

	Video Game Players	Non-Video Game Players
Number of Participants	28	19
Average Age (years)	20.64 ± 2.45	19.94 ± 2.62
Males	24	7
Females	4	12
Right-Handed	26	17
Left-Handed	2	2

2.1.2 Experiment Task, Stimuli and Design

Before their scheduled MRI scan session, participants were shown a demonstration of the task they would be completing, and all questions pertaining to the task were answered. The decision-making task for this experiment was a moving dots (MD) left-right discrimination task modified from the previous version (Chand & Dhamala (2016)). Participants would be cued for a color to attend to on the next screen. The cue was a text prompt that spelled out the color, and the font color was the same color to avoid confusion. On the next screen, participants would see two different sets of overlapping dots (each set consisting of 600 dots) going in opposite directions. Participants would then respond whether they thought the dots of the cued color were going left or right using a controller inside the fMRI. Participants were told to respond as quickly and accurately as possible for which direction they thought the colored set of dots they had been cued for were going. Participants were informed of the total time of the scan session, safety protocols, and given an emergency button to reduce anxiety inside the fMRI. Participants were asked to lay still and not to move during the scan

periods. All motion movements were monitored during scan sessions, and participants were notified if they began to move too much.

The direction of the cued set was randomized between each MD task, and the colors of the two sets were randomly picked from a list of preset groupings as shown in Figure 2.2. These difficulty pairings were based on the color wheel; easy difficulty level was between two primary colors, medium was between primary and secondary colors, hard was a primary or secondary color versus a tertiary color. The speed setting went from 0 (No-Motion) to 4, the fastest setting. These settings were determined from finding the max speed of the dots before illusory motion reversal became possible and using points every quarter of the max speed for lower speed settings.

For each task period, the difficulty and speed setting of the task was randomly chosen for that period. Within each task period, participants would respond to a total of 3 MD tasks totaling 15 seconds. To respond, participants would indicate if the dots were moving left, right, or not at all by pressing the left or right buttons with their thumbs or no button press at all if no-motion. After the task period, there was a rest period of 15 seconds before the next task period began with a new difficulty and speed setting. Figure 1 shows the experiment design and timescale. Each combination of speed and difficulty setting appeared four times for each participant's scan session for a total of 60 task periods. All scan sessions followed this same design. The task sequence was designed in and displayed by the PsychoPy stimulus software (Peirce et al. (2019)).

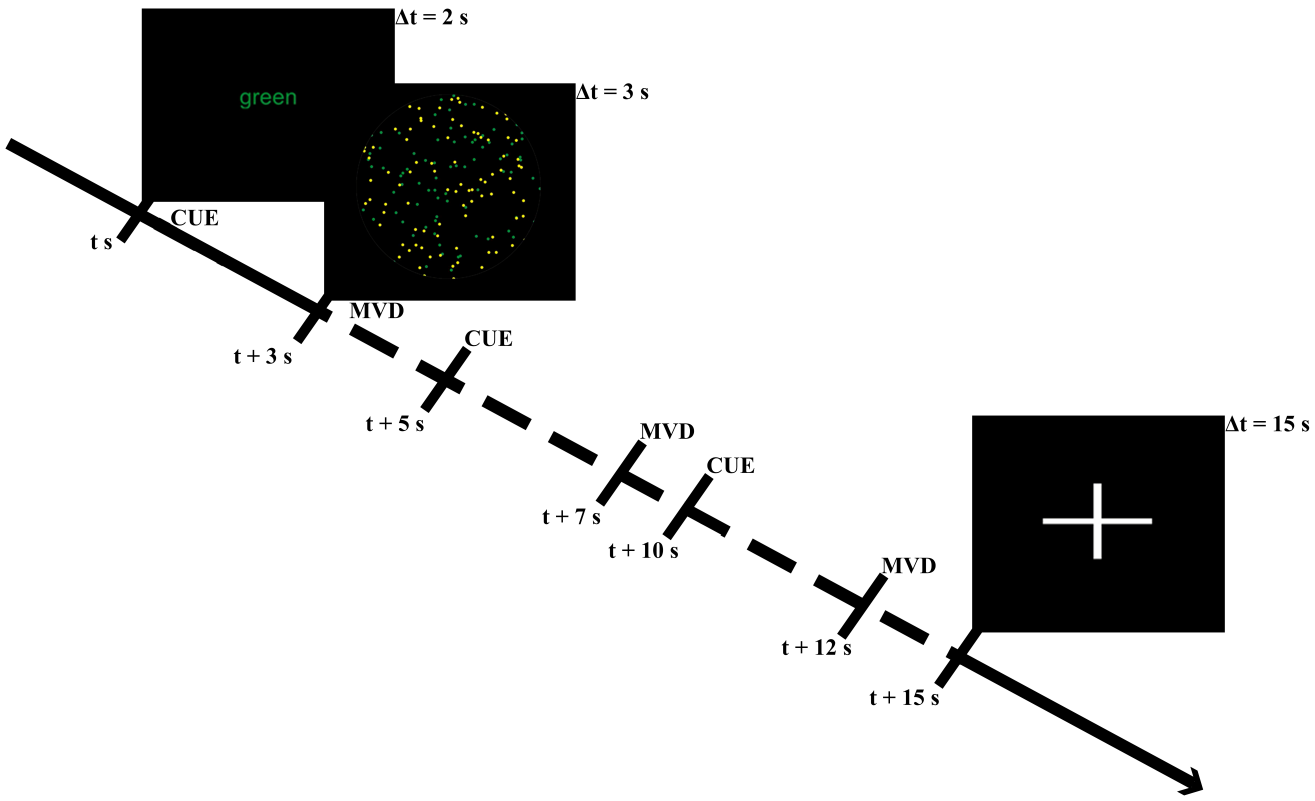

Figure 2.1 Task started with a cue for which color to attend to on the next screen. After 2 seconds, the MD would appear in the same location and participants would have 3 seconds to respond. After the 3 second response window, the next cue would appear and begin the stimulus period of 5 seconds total. The task appeared a total of 3 times per task block for a total of 15 seconds of task and then immediately followed by a 15 second rest.

2.2 Data Collection

2.2.1 Behavioral Data

Behavioral data was collected by the stimulus software, PsychoPy (Peirce et al. (2019)), and the computer running the software. Participant's decisions via button presses and response times were recorded for each MD task. Participant's left/right decisions were translated into participant accuracy scores. Participants had to respond correctly to the MD

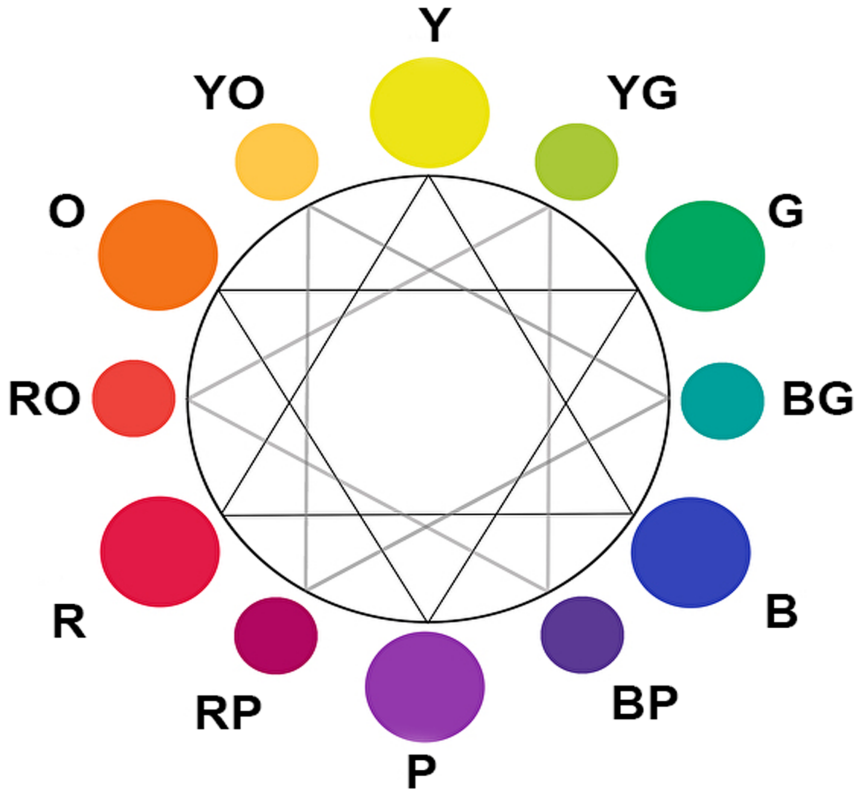

Difficulty Level	Color Pairing
Easy	R-B, R-Y, B-Y
Medium	R-O. R-P, B-P, B-G, Y-O, Y-G
Hard	R-RO, R-RP,Y-YO,Y-YG,B-BP,B-BG,O-RO,O-YO,P-RP,P-BP,G-YG,G-BG

Figure 2.2 All possible pairs of color combinations divided into difficulty rank based on contrast as defined by color wheel.

within the stimulus period to be considered correct answers. Responses after the stimulus ended, incorrect responses, and no response at all for any condition other than no-motion were considered incorrect answers. The correct responses would then be divided by the total number of tasks and multiplied by 100 to give each participant a percentage score, which

was their task accuracy score. Response times were taken as the time from the MD onset after the text cue. Participants had to respond within 3 seconds of the MD onset.

2.2.2 Structural and Functional MRI Brain Data

Whole-brain structural and functional MR imaging was conducted on a 3 Tesla Siemens Magnetom Prisma MRI scanner at the joint Georgia State University and Georgia Institute of Technology Center for Advanced Brain Imaging, Atlanta, Georgia. First, high-resolution anatomical images were acquired for voxel-based morphometry and anatomical reference using a T1-MEMPRAGE scan sequence (TR = 2530 ms, TE1-4: 1.69-7.27 ms, TI = 1260 ms, Flip Angle = 7 deg, Voxel size 1 mm x 1 mm x 1 mm). Following, four functional scans were acquired using a T2*-weighted gradient echo-planar imaging sequence while participants completed the behavioral task (TR = 535 ms, TE = 30 ms, Flip Angle = 46 degrees, Field of View = 240 mm, Voxel Size = 3.8 mm x 3.8 mm x 4 mm, Number of slices = 32 collected in an interleaved order, Slice thickness = 4 mm). Each scan run was 7 minutes and 30 seconds long, for a total functional scan time of 30 minutes, translating into 3,440 brain images.

2.3 Data Analysis

2.3.1 Data Preprocessing

All fMRI data was preprocessed using the Statistical Parametric Mapping Matlab software suite (SPM12, Friston (2010)). Data was first imported from DICOM format into NIFTI, then slice time corrected, realigned for motion correction, and realigned for field distortion using fieldmap corrections. Each participant's data was then co-registered to their

anatomical image and normalized to a Montreal Neurological Institute (MNI) template. The anatomical image was then segmented. Lastly, the normalized data was spatially smoothed with an 8 mm isotropic Gaussian kernel.

2.3.2 Task-Related Brain Activation

Task-related activations were computed by using the two-level random-effects analysis approach (Friston (2010)). For the first-level analysis, data was analyzed using a mass univariate approach based on general linear models (GLMs). The GLM was defined as $y = \beta X + \epsilon$, where y is the observed data, β is a matrix of regression parameters, X is the design matrix constructed from the stimulus and task sequence and participant's movements, and ϵ is the residual error. The GLM design matrix was specified for each participant based on when a specific task condition would have appeared for them over four runs. The specified task conditions were: Easy Speed 0 (E0), Easy Speed 1 (E1), Easy Speed 2-3 (E23), Easy Speed 4 (E4), Medium Speed 0 (M0), Medium Speed 1 (M1), Medium Speed 2-3 (M23), Medium Speed 4 (M4), Hard Speed 0 (H0), Hard Speed 1 (H1), Hard Speed 2-3 (H23), Hard Speed 4 (H4) and four motion regressors. Contrast images for Task - Rest and Motion - No-Motion were created for each participant. The contrast images of t-maps were put in a second-level analysis for a two-sample t-test to assess overall group effects and group differences. The results were thresholded using family-wise error rate at corrected $p < 0.05$ and cluster size $k > 20$ voxels to compute brain activation maps for both contrasts.

2.3.3 Brain Regions of Interest (ROI) selection

Three sets of Regions of Interest (ROI) were used. The first set was based on our group (VG and NVG) activation maps. The second and third sets were based on previous works in decision-making network interactions and network interactions in young adults, respectively.

2.3.3.1 Task Related Regional Activity

ROI were defined using 2nd-level analysis activation results for all participants. Activation clusters were identified for family-wise error (FWE) corrected $p < 0.01$ and cluster extent $k > 20$. Coordinates for peak cluster activations were recorded and used in the Pick-Atlas (Maldjian et al. (2003)) to determine the regions they correlated with. Table 2.2 shows all ROI selected and for task condition. Regional average percent signal change for each condition specified in the 1st-Level per run was extracted from each ROI using MarsBaR (Brett et al. (2002)) for each condition in the GLM design. ROI were resampled to Talairach space using AFNI's 3dresample, and then voxel-wise BOLD time-series was extracted using AFNI's 3dmaskdump (Cox (1996), Cox & Hyde (1997)).

2.3.3.2 Decision Making Related Network

In Chand & Dhamala (2016), three networks, Central Executive Network (CEN), SN, and Default Mode Network (DMN), were examined, using coordinates from Sridharan et al. (2008), to see how they interacted for perceptual decision making tasks. We created 6 mm spherical masks around the coordinates given in Sridharan et al. (2008). Using the same method as above, we extracted time-series data for each ROI. Table 2.3 shows the coordinates

for each ROI center point.

2.3.3.3 Attention Switching Interactions

In Zhou et al. (2017), three networks, Dorsal Attention Network (DAN), DMN, and SN, were examined to see how they interacted for young adults switching between resting and task. We created 6mm spherical masks around the coordinates given in Zhou et al. (2017). Using the same method as above, we extracted time-series data for each ROI. Table 2.3 shows the coordinates for each ROI center point.

2.3.4 ROI specific Percent Signal Change

Regional Percent Signal Change data was averaged for each participant across all 4 task runs to obtain participant averages per ROI per task condition. For each participant, the average percent signal change for each difficulty level and speed setting was calculated. A two-sample t-test was used to determine the statistical significance of group percent signal change differences for each difficulty setting and speed setting for $p < 0.05$.

2.3.5 Functional Connectivity

Time-series data was normalized for each participant per ROI by taking out the temporal means and dividing by the standard deviation. The normalized time-series for each participant were averaged across all voxels to calculate the average time-series per participant per ROI. The time-series were segmented based on each task condition occurrence for each participant. Segmented time-series data were corrected for any linear trends. Pearson correlation coefficients were calculated for all pairs of ROI for each group of participants creating a

functional connectivity (FC) matrix. Correlation coefficients, r, were transformed to z-score using the Fisher Transformation, $z = arctanh(r)$. A two-sample t-test was used on the group z-scores to determine significant functional connections at $p < 0.05$, for group differences. Z-scores were transformed back using the inverse Fisher Transformation, $r = tanh(z)$. The significance of the correlation was estimated using the student's t cumulative distribution function for each connection.

2.3.6 Directed Functional Connectivity

2.3.6.1 Granger Causality

Time-series data for Granger causality (GC) calculations were normalized, voxel averaged, segmented, and detrended the same as FC time-series data. All participants' data were combined along the second dimension as trials to calculate the proper model order in parametric modeling for GC calculations. Once the model order was determined, GC matrices were computed for each participant using the conditional Granger causality (CGC)(Dhamala et al. (2008),Wen et al. (2013)). Conditional Granger causality calculates the direct causal influences from region X to region Y using the equation:

$$I_{Y \to X|Z}(f) = ln \frac{\Omega_{xx}}{Q_{xx}(f)\Sigma_{xx}Q^*_{xx}(f)} \tag{2.1}$$

where Σ_{xx} is the covariance of the trivariate autoregressive model and,

$$Q(f) = \begin{pmatrix} Q_{xx}(f) & Q_{xy}(f) & Q_{xz}(f) \\ Q_{yx}(f) & Q_{yy}(f) & Q_{yz}(f) \\ Q_{zx}(f) & Q_{zy}(f) & Q_{zz}(f) \end{pmatrix} = G(f)^{-1} \cdot H(f) \tag{2.2}$$

where the quantities $G(f)$ is the transfer function matrix for the joint autoregressive

model for X_t and Z_t and $H(f)$ is the transfer function matrix for the trivariate autoregressive model for X_t, Y_t and Z_t.

If $f_{Y\to X|Z}(f) > 0$ then Y is said to have a direct causal effect on X. If $f_{Y\to X|Z}(f) = 0$ then the causal effect of Y on X is said to be mediated entirely by a third region or not present at all. The equivalent time-doman CGC is:

$$F_{Y\to X|Z} = \frac{2}{f_s}\int_0^{f_s} I_{Y\to X|Z}(f)df \tag{2.3}$$

where f_s is the sampling frequency. This can be interpreted as taking the joint flow from YZ and subtracting the flow from Z:

$$F_{Y\to X|Z} = F_{YZ\to X} - F_{Z\to X} \tag{2.4}$$

See Appendix C for some more details on the method. CGC noise threshold was calculated using a random permutation technique as described in Brovelli et al. (2004) for 1000 permutations. Significant group GC differences were calculated using the Mann-Whitney U-test. Thresholding the group GC matrices by both the noise threshold and significant GC connections as determined by Mann-Whitney U-test removed all non-significant GC for both groups.

2.3.6.2 Net Information Flow

Using group GC matrices, net information flow was calculated for each mth ROI. First, all connections from ROI_X to all other ROI were summed up to obtain ROI_X's outflow.

$$outF(m) = \frac{1}{N-1}\sum_{i=1}^{N} F_{m\to i} \tag{2.5}$$

Next, all connections from all other ROI to ROI_X were summed and then the negative of the summation to obtain ROI_X's inflow.

$$inF(m) = \frac{1}{N-1}\sum_{i=1}^{N} F_{i\to m} \tag{2.6}$$

The inflow and outflow of ROI_X were then summed together to determine if that region acted more as a "source", outflow greater than inflow, or as a "sink", inflow greater than outflow, for each group. Inflow, Outflow, and Netflow were compared between groups using Mann-Whitney U-test.

2.3.6.3 Brain Behavior Relation: Granger Causality vs Response Time

Granger Causality values for each participant per connection were plotted against participant response time (RT) to look for correlations between performance and connectivity strength. A linear fit, thresholded at $p < 0.05$, was used to calculate correlation coefficients between GC and RT.

2.3.7 Voxel-Based Morphometry

Structural data was analyzed with FMRIB Software Library Voxel-Based Morphometry (FSL-VBM) (Douaud et al. (2007), `http://fsl.fmrib.ox.ac.uk/fsl/fslwiki/FSLVBM`), an optimized VBM protocol (Good et al. (2001)) carried out with FSL tools (Smith et al. (2004)). First, structural images were brain-extracted and grey matter-segmented before being registered to the MNI 152 standard space using non-linear registration (Andersson & Smith (2007)). The resulting images were averaged and flipped along the x-axis to create a left-right symmetric, study-specific grey matter template. Second, all native grey matter images and ROI masks were non-linearly registered to this study-specific template and "modulated" to correct for local expansion (or contraction) due to the non-linear component of the spatial transformation. The modulated grey matter images were then smoothed with an isotropic Gaussian kernel with a sigma of 3 mm. Finally, voxelwise GLM was applied using permutation-based non-parametric testing and atlas-based ROI mask, correcting for multiple comparisons across space. For this analysis, we chose to use Harvard-Oxford cortical and subcortical structural atlas (Desikan et al. (2006)) based ROI to get whole region grey matter calculations instead of reducing it down to the 6mm spheres used in previous analyses.

Table 2.2 Regions of Interest for Brain Activations

Contrast	Region of Interest	MNI Coordinates			T
		x(mm)	y(mm)	z(mm)	
Task - Rest	Left Calcarine	-6	-93	-10	18.27
	Right Middle Cingulate	6	17	42	14.67
	Right Inferior Frontal Orbital	25	29	-6	14.53
	Right Inferior Frontal Triangularis	44	17	26	14.26
	Right Hippocampus	25	-28	-2	14.43
	Left Insula	-28	21	2	14.54
	Right Insula	36	21	2	16.13
	Right Lingual	21	-82	-14	19.74
	Left Midbrain	-6	-28	-6	13.59
	Right Midbrain	6	-28	-6	14.21
	Right Superior Occipital	17	-93	6	18.2
	Left Inferior Parietal	-44	-40	42	14.94
	Left Inferior Parietal 2	-28	-51	46	14.9
	Right Inferior Parietal	32	-51	46	13.16
	Right Precentral	48	10	34	12.96
	Right Putamen	17	13	-2	13.45
	Left Supplementary Motor Area	2	10	50	14.77
	Left Thalamus	-13	-6	-2	12.94
Motion - No-Motion	Right Calcarine	13	-89	-2	9.07
	Left Middle Occipital	-25	-89	14	7.49
	Right Middle Occipital	40	-66	6	5.97
	Left Superior Occipital	-21	-89	22	7.04
	Left PostCentral	-47	-25	46	5.93
	Right Supplementary Motor Area	10	6	50	6.63
	Left SupraMarginal	-47	-25	34	5.34
	Vermis 9	2	-59	-38	7.55

Brain Activation ROI for Task - Rest and Motion - No-Motion contrasts corrected for multiple comparisons. All regions are under statistical significance of FWE corrected for multiple comparisons at $p < 0.01$ and cluster extent $k < 20$.

Table 2.3 Regions of Interest for Network Interactions

Network Interaction	Region of Interest	MNI Coordinates			Network
		x(mm)	y(mm)	z(mm)	
CEN-DMN-SN	DLPFC	45	16	45	CEN
	lPPC	-38	-53	45	CEN
	rPPC	54	-50	50	CEN
	PCC	-7	-43	33	DMN
	VMPFC	-2	36	-10	DMN
	ACC	4	30	30	SN
	lAI	-32	24	-6	SN
	rAI	37	25	-4	SN
DAN-DMN-SN	aMPFC	3	54	18	cDN
	lAG	-48	-69	33	cDN
	PCC	-3	-57	21	cDN
	rAG	51	-63	27	cDN
	lFEF	-24	-9	57	DAN
	lIFG	-51	9	27	DAN
	lIPS	-42	-36	45	DAN
	rFEF	27	-3	54	DAN
	rIFG	54	12	30	DAN
	rIPS	39	-42	51	DAN
	dACC	-3	15	42	SN
	lAI	-36	15	6	SN
	laPFC	-27	45	30	SN
	rAI	33	18	6	SN
	raPFC	30	42	30	SN

All ROI spheres were based on previous studies (Chand & Dhamala (2016), Sridharan et al. (2008), Zhou et al. (2017)).

CHAPTER 3
RESULTS

3.1 Behavioral Performance

Both groups showed increased response time for hard difficulty level and low speed, speed setting 1. For all conditions and overall performance, VGP had faster response times and higher accuracy than NVGP. VGP were significantly more accurate than NVGP for overall task performance ($2.24 \pm 6.87\%$), easy condition tasks ($7.12 \pm 5.38\%$) , and speed 2 condition tasks ($4.13 \pm 14.14\%$). All response times regardless of condition were significantly lower in VGP than NVGP with an average difference of 190 milliseconds (ms) (VGP = 926.75 ± 424.71, NVGP = 1115.93 ± 483.89). Figure 3.1 & Table 3.1 show all results for behavioral task performance. For all bar graphs, dark green and dark orange correspond to VGP and NVGP, respectively.

3.2 ROI Signal Changes

The contrasts used were Task vs. Rest and Motion, all tasks with speed 1 or greater, vs. No Motion, all tasks with speed 0 for all participants together. This gave an activation map with all regions that both groups utilized for task performance. From this activation map, 6 mm spheres were placed around the local maxima peak voxel coordinates and extracted percent signal change from baseline using MarsBaR (Brett et al. (2002)). We compared group percent signal change from these regions and found ten regions where VGP and NVGP significantly differed. Of these regions, only one showed higher activation in NVGP compared

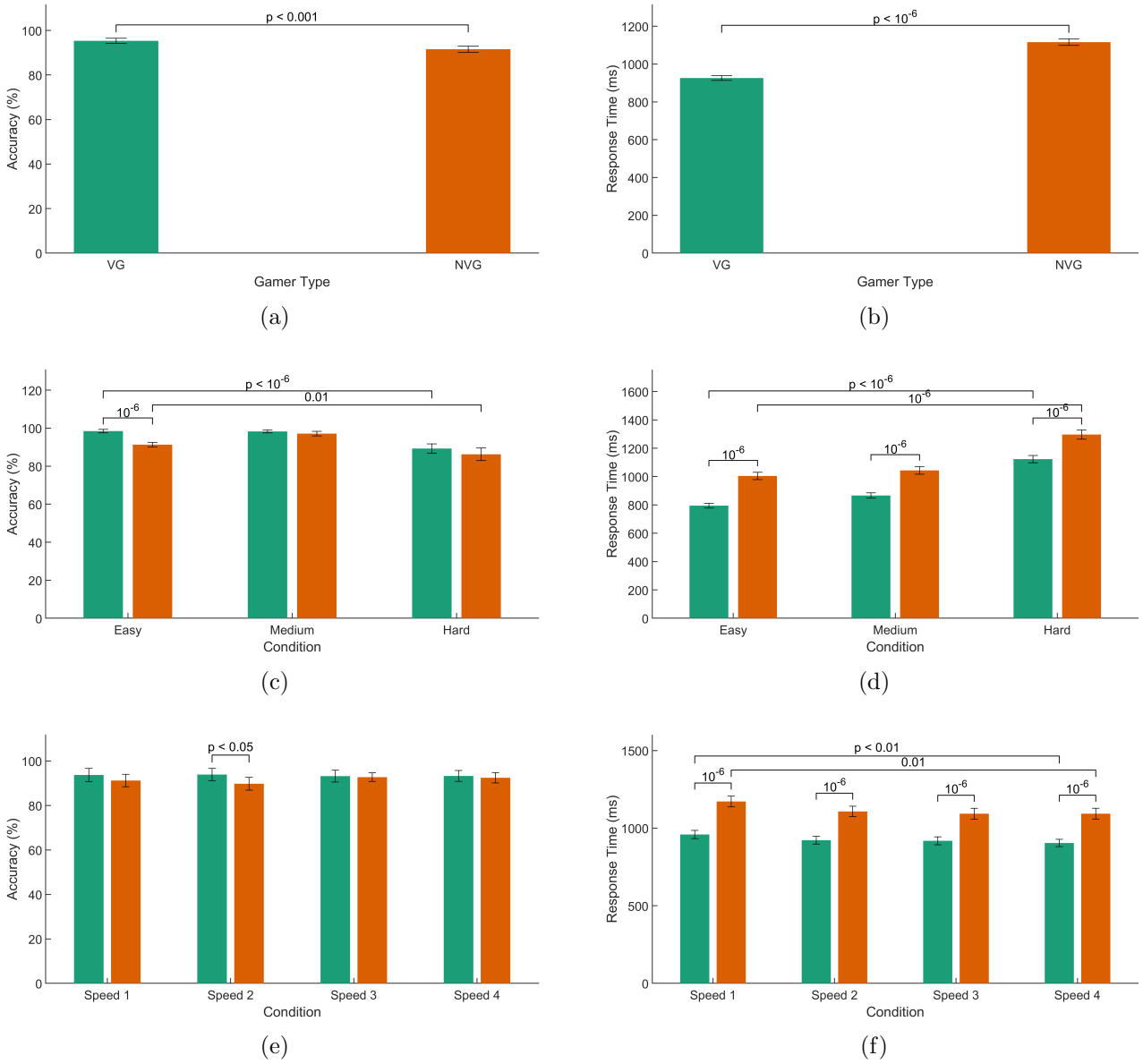

Figure 3.1 Behavioral task performance results. Sub-figures 3.1a & 3.1b are for overall task performance. Sub-figures 3.1c & 3.1d are for task performance by difficulty level setting. Sub-figures 3.1e & 3.1f are for task performance by speed setting

to VGP, and all other ROI favored VGP. Figure 3.2 shows all regions found to be significantly different.

Figure 3.3 and 3.4 shows all regions found to be significantly different based on difficulty

Table 3.1 Behavioral MD Performance Results

Condition	VGP	NVGP	p
General	95.26 ± 3.93	93.016 ± 5.63	0.0008
	925.61 ± 432.18	1117.23 ± 494.78	2.05e−70
Hard	89.29 ± 7.98	86.25 ± 12.45	0.16
	1123.07 ± 505.45	1296.59 ± 539.06	2.14e−16
Medium	98.29 ± 2.58	97.12 ± 4.56	0.13
	866.34 ± 375.77	1043.51 ± 447.21	4.65e−27
Easy	98.45 ± 2.98	91.33 ± 4.48	1.68e−14
	794.68 ± 329.14	1004.24 ± 418.41	1.68e−43
Speed 1	93.7 ± 9.7	91.2 ± 10.53	0.22
	959.10 ± 456.53	1171.82 ± 492.91	1.35e−21
Speed 2	93.89 ± 9.03	89.76 ± 10.88	0.04
	922.33 ± 426.98	1107.68 ± 479.04	1.28e−18
Speed 3	93.19 ± 8.75	92.72 ± 7.31	0.77
	918.43 ± 441.24	1093.07 ± 491.55	9.56e−16
Speed 4	93.26 ± 8.07	92.44 ± 8.77	0.63
	904.48 ± 407.16	1093.29 ± 499.5	1.77e−19

Group task performance averages for all difficulty level and speed settings.

and speed, respectively. These regions are left and right Supplementary Motor Area (SMA), left and right Midbrain (MB), right Putamen (PUT), right Lingual Gyrus (LING), left Inferior Parietal Lobe (IPL), left Middle Occipital Gyrus (MOG), right Inferior Frontal pars triangularis (IFT), Vermis 9 (V9), left Thalamus (THA), right Hippocampus (HPC).

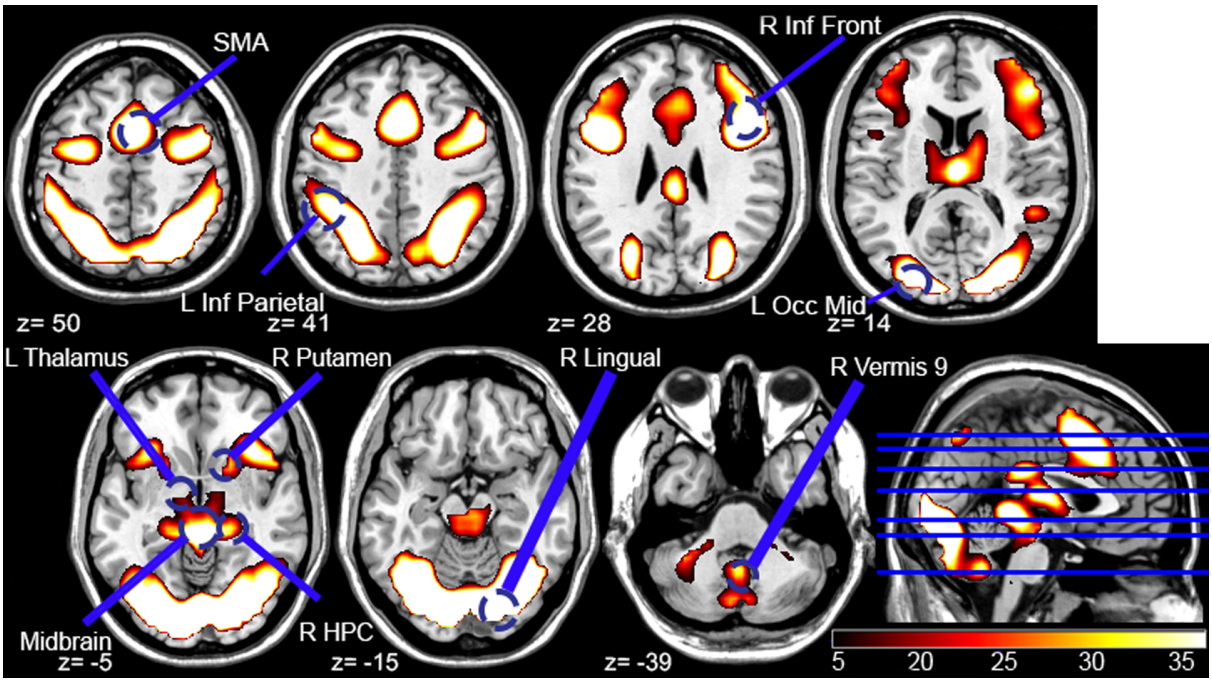

Figure 3.2 Activation map for all participants at corrected significance $p < 0.05$ (FWE), the ROI named and circled here were shown to have significantly percent signal change between VGP and NVGP.

3.3 Undirected and Directed Functional Connectivity

3.3.1 Task Related Regional Brain Activity

Undirected FC analysis was performed for all nodes, and we found that only six connections were significantly different between groups. These connections are non-directional and only show an overall correlation between the two regions. For all connections, VGP had higher correlations, and therefore higher connectivity, than NVGP. For 3 of the connections, NVGP showed no connectivity between these regions. Figure 3.5 shows the significant functional connections for VGP (top left panel) and NVGP (top right panel), and a comparison of the connectivity coefficients (bottom panel).

CGC analysis was used to assess directional connectivity between two regions, two in-

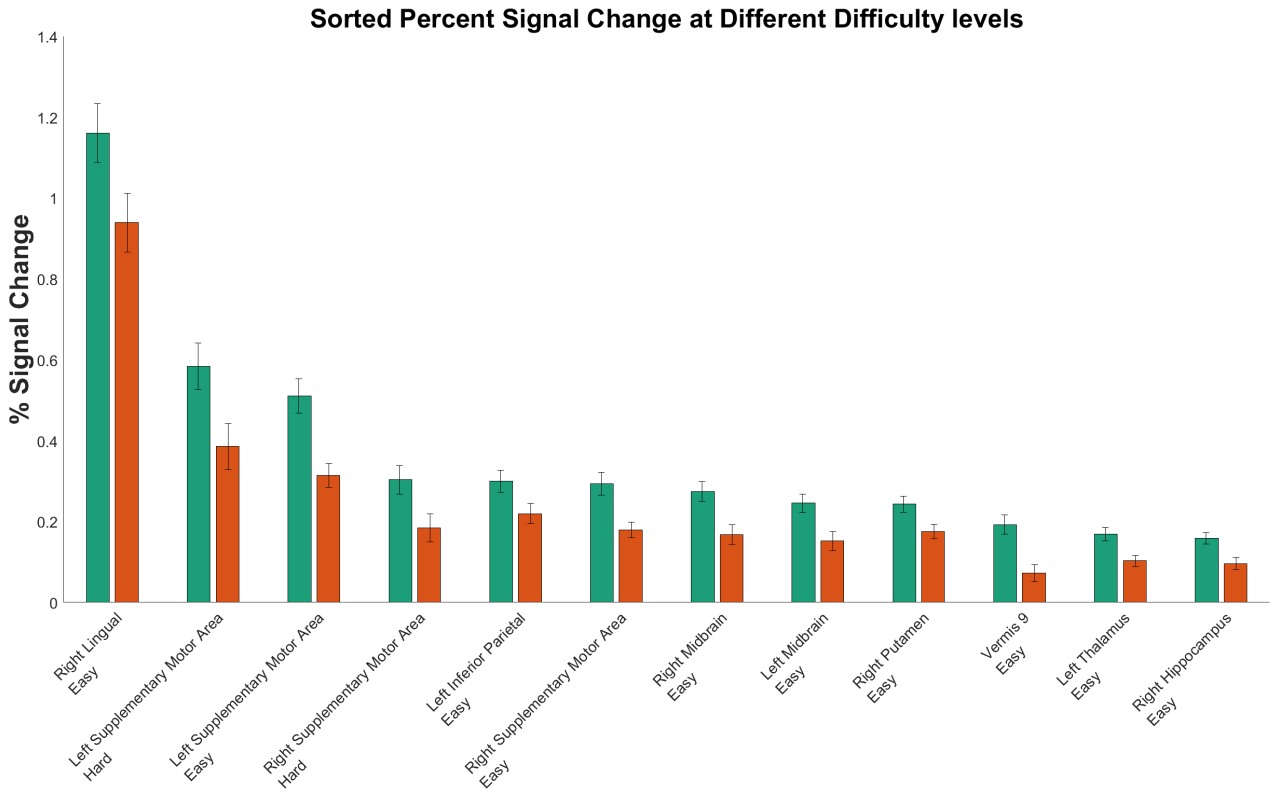

Figure 3.3 Histogram of all regions found to have significantly different percent signal change between groups based on difficulty setting.

dividual path interactions between these regions, one going from ROI_X to ROI_Y and vice versa for the other. This analysis was done for all conditions together as we were looking for differences between groups overall and not for specific conditions. The CGC connections were thresholded for noise, compared between groups to find significant connection differences, and then focused on connections where VGP were significantly higher, $p < 0.01$, and any significant connections, $p < 0.05$, from dorsolateral Prefrontal Cortex (DLPFC). A total of 4 connections were found to be higher in VGP. Figure 3.6 shows the connections that were significantly higher for VGP. Figure 3.7 shows the connections for DLPFC that were

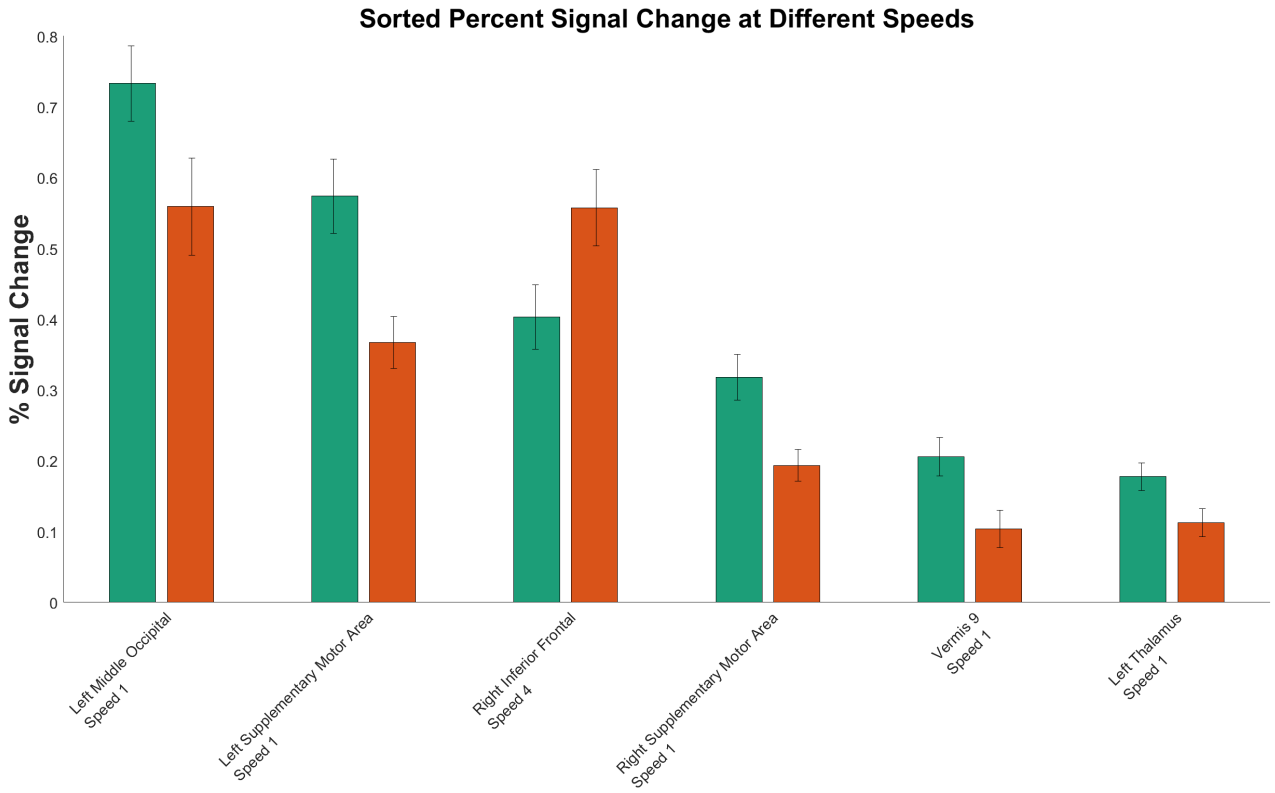

Figure 3.4 Histogram of all regions found to have significantly different percent signal change between groups based on speed setting.

significantly higher for VGP. The node that the arrow points toward is the node receiving causal influence from the other node. All other connections were found to have no significant differences between groups.

3.3.2 Central Executive - Default Mode - Salience Networks

FC analysis was conducted on eight nodes to observe if VGP had modulated connections between specific regions corresponding to specific networks as shown in Table 2.3. For these network interactions, only two connections were found to have significant differences, but only one was present in NVGP. Similar to the activation-based ROI, both connections had

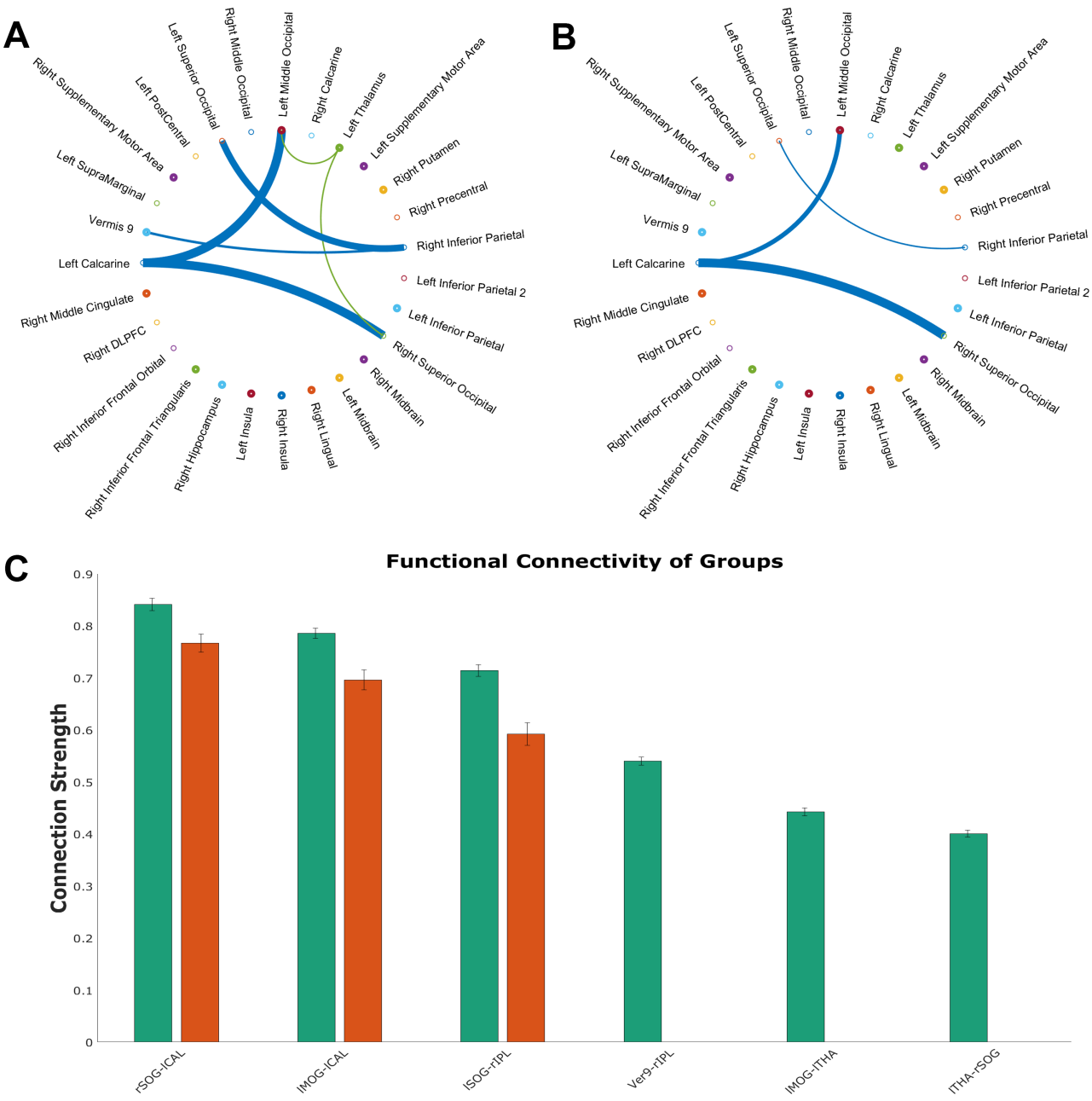

Figure 3.5 Significant Functional Connections. Line thickness indicates strength of connection, thicker line = higher connectivity and vice versa. A: Significant connections for VGP. B: Significant connections for NVGP. C: Comparison between significant connections in both groups, dark green for VGP and dark orange for NVGP

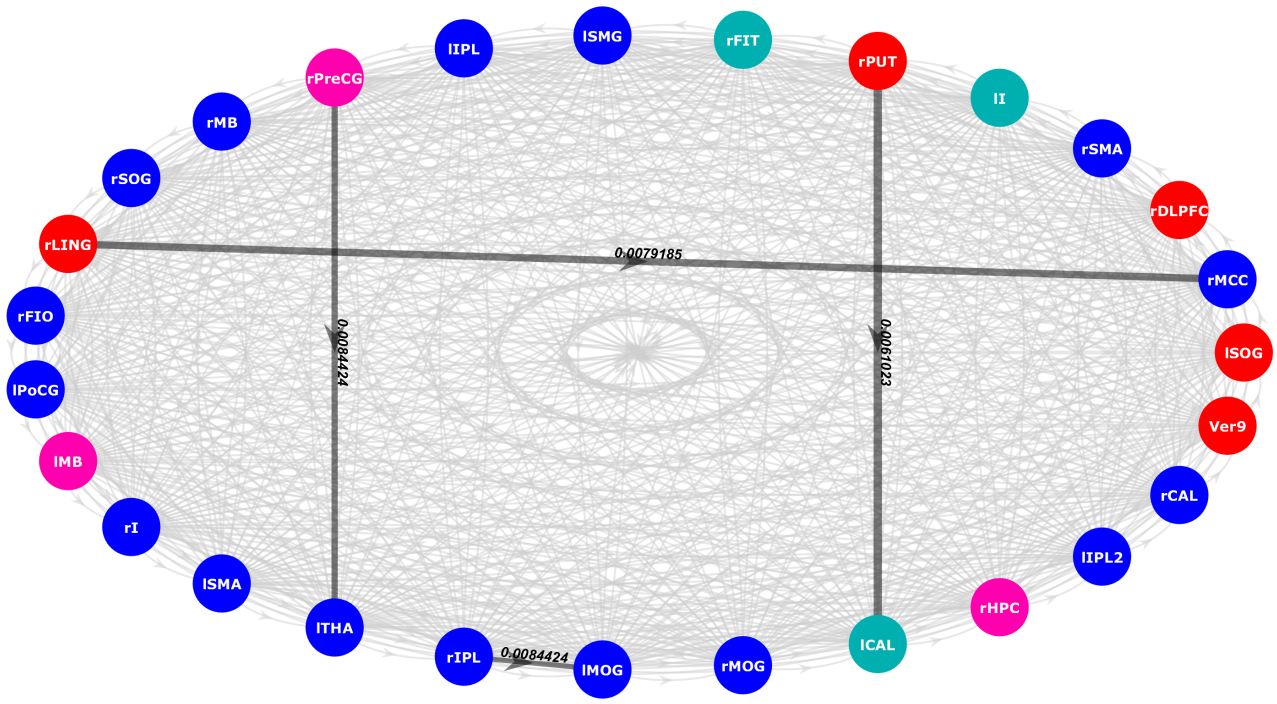

Figure 3.6 Significant functional connections that were higher in VGP. Corresponding GC values are displayed along the line. Color of the nodes corresponds to source or sink behavior of the region. Blue corresponds to sink behavior for both groups. Red corresponds to source behavior for both groups. Light blue corresponds to regions that were sink for VGP and source for NVGP. Pink corresponds to regions that were source for VGP and sink for NVGP.

higher values for VGP. Figure 3.9 shows the connections found to be significantly different between groups. Functional connectivity results for VGP and NVGP are shown in the top left and right panels, respectively. A comparison bar graph of these connectivity results is in the bottom panel.

Following the FC analysis, CGC analysis was then performed on the same nodes as established above. After thresholding for noise and significance, we found that only one connection, Posterior Cingulate Cortex (PCC) to left anterior Insula (aI), was significantly different between the groups. Figure 3.10 show this connection with the arrow pointing

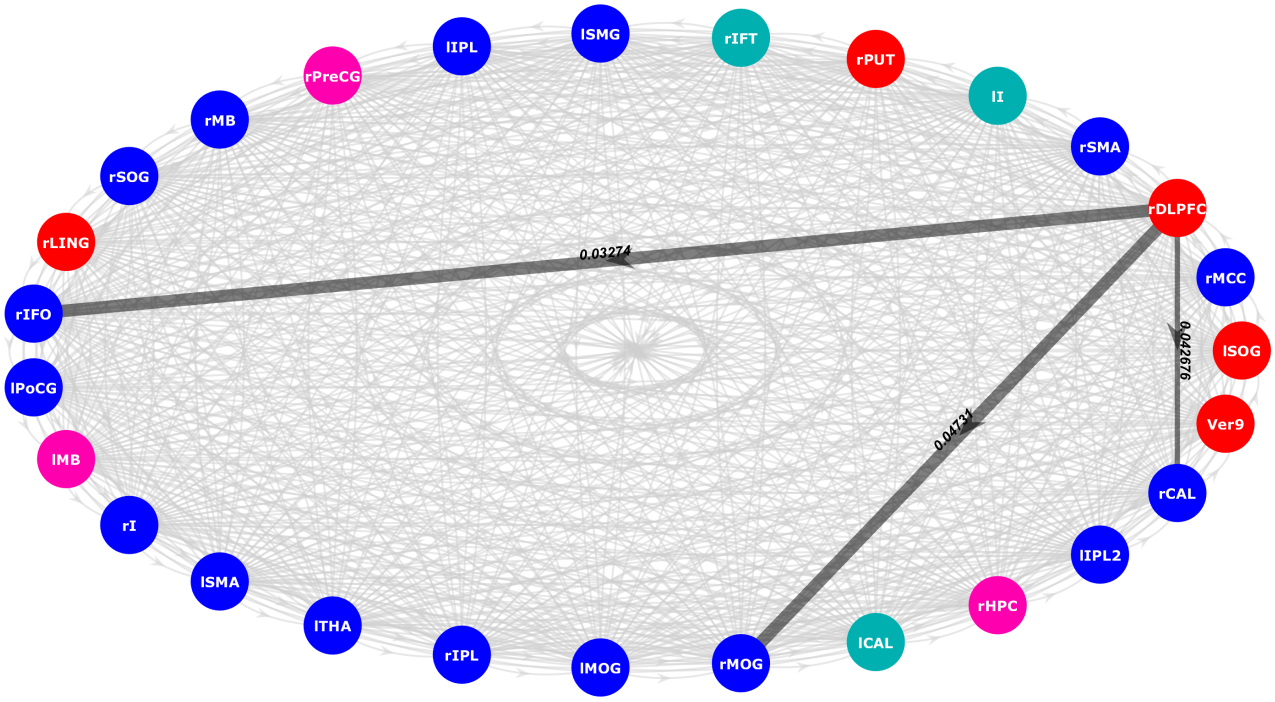

Figure 3.7 Significant functional connections higher in VG players that involved DLPFC. Corresponding GC values are displayed along the line.

towards the node receiving causal influence. All other connections we found to have no significant differences.

The GC values from each region in one network to each region in another specific network were averaged to find the average GC from one network to another, i.e., CEN to SN. We found that five of six connections between these networks were significantly different between groups. Figure 3.12 shows the between network connections that were significantly higher for VGP and NVGP, respectively.

3.3.3 Dorsal Attention-Default Mode-Salience Networks

FC analysis was conducted on 15 nodes as shown in Table 2.3. The connections from regions in one network to another were taken for both groups and compared using a t-test. We then averaged those connections to obtain the average connectivity between the two networks, i.e., SN and DMN. We found that there was a significant difference between groups for connectivity between DMN and DAN. Figure 3.14 shows the connection found to be significantly different between groups.

Following the FC analysis, CGC analysis was then performed on the same nodes as established above. After thresholding for noise and significance, we found that eleven connections were significantly different between the groups. Of these eleven, only five we significantly higher for VGP; the remaining significant connections were higher in NVGP. Figures 3.16 & 3.15 show these connections with the arrow pointing towards the node receiving causal influence. Figure 3.16 shows the connections found to be higher for VGP. Figure 3.15 shows the connections found to be higher for NVGP. All other connections we found to have no significant differences.

Similar to the FC analysis, we compared the connections from regions in one network to regions in another using MWU. It was found that five of six connections between these networks were significantly different between groups. Figure 3.17 shows the between network connections that were significantly higher for VGP and NVGP, respectively.

3.4 Brain Network Source & Sink Activities

3.4.1 Task Related Regional Brain Activity

Information flow analysis was performed for all ROI. We found that six regions had significantly different informational flows. For net flow, three regions were found to have significant differences between groups: right Middle Cingulate (MCC), right Precentral Gyrus (PreCG), and left Superior Occipital Gyrus (SOG). Figure 3.20 displays the net flow from each ROI; the ROIs with significant differences are in bold and have dark green and dark orange bars on the plot.

3.4.2 Central Executive - Default Mode - Salience Networks

Information flow analysis was performed on each node. We compared differences for inflow and outflow from each ROI between groups. We found that only one region had a significant difference. The outflow from the Posterior Parietal Cortex (PPC) was greater in NVGP than in VGP. Figure 3.21 shows the inflow and outflow from each ROI; the significant ROI is in bold and has dark green and dark orange bars.

3.5 Brain Behavior Relation: Granger Causality vs Response Time

Lastly, significant GC values were correlated to RT to see how the neural differences related to behavioral performance. This was only done for connections that were found to have a significant GC difference between groups.

3.5.1 Task Related Regional Brain Activity

For region-to-region connectivity, we found that two connections had moderate correlations between GC and RT, left Postcentral Gyrus (PoCG) to left IPL (r = -0.356, p = 0.03) and right PreCentral Gyrus (PreCG) to left SMA (r = -0.4, p = 0.01). We saw a positive and negative relation for left PoCG to left IPL and right PreCG to left SMA, respectively. Figure 3.8 shows the correlation scatter plots for these connections.

3.5.2 Central Executive - Default Mode - Salience Networks

In the CEN-DMN-SN network interactions, we looked at both individual region-to-region significant connections and significant connections between networks. We found that for the one connection, PCC to left aI, response time decreased as the connectivity strength increased. Next, we looked to examined this correlation between network interactions that saw were significantly different. We found that two connections had moderate correlations between GC and RT both coming from SN, SN to CEN (r = 0.398, p = 0.006) and SN to DMN (r = 0.352, p - 0.01). Both connections showed that as GC increased, so did RT. Figure 3.11 shows the correlation scatter plot for the PCC to left aI connection. Figure 3.13 shows the correlation scatter plots for the network-to-network connections connections.

3.5.3 Dorsal Attention-Default Mode-Salience Networks

Lastly, for DAN-DMN-SN network interactions, we examined both region-to-region significant connections and between network connections. We found that one ROI-to-ROI connection and one between network connection correlated with RT. The connections that had

moderate correlations between GC and RT were anterior Medial Prefrontal Cortex (aMPFC) to dorsal anterior Cingulate Cortex (dACC) (r = -0.34, p = 0.01) and DAN to SN (r = -0.34, p = 0.02). Both correlations showed that as GC increased, RT decreased. Figure 3.19 shows the correlation scatter plot for the aMPFC to dACC connection. Figure 3.19 shows the correlation scatter plot for the between network connection.

3.6 Brain structural changes with Voxel-Based Morphometry

Results for VBM analysis results were thresholded at significance $p < 0.05$. Five regions were found to have significantly different Grey Matter Volumes (GMV) for the activation-based ROI and one region for DAN-DMN-SN Network: left/right Insula, right Occipital Lobe, right PUT, right SMA, and left Angular Gyrus (AG). Table 3.2 shows relevant statistics, coordinates for peak difference voxel, and which group had higher GMV. Figure (3.22 shows the ROI masks used and where they were located.

Region of Interest	p	MNI Coordinates			Z	Higher Group
		x(mm)	y(mm)	z(mm)		
Left Insula	0.022	-38	-10	-10	3.91	VG
Right Insula	0.006	38	-4	-8	4.62	VG
Right Occipital	0.038	14	-100	6	4.51	NVG
Right Putamen	0.007	34	-4	-10	4.47	VG
Right SMA	0.043	8	-10	56	3.5	VG
Left Angular	0.035	-48	-62	-16	3.6	VG

Table 3.2 ROI Voxel-Based Morphometry Results.

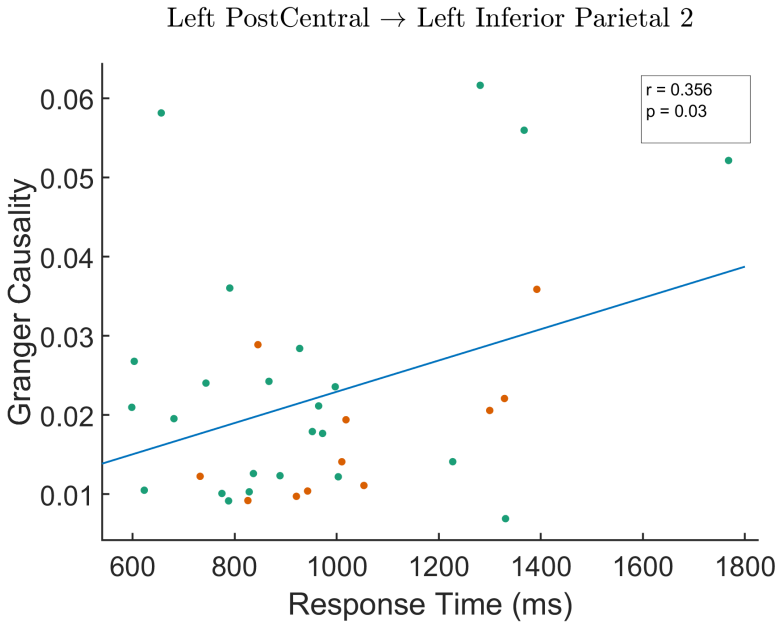

(a)

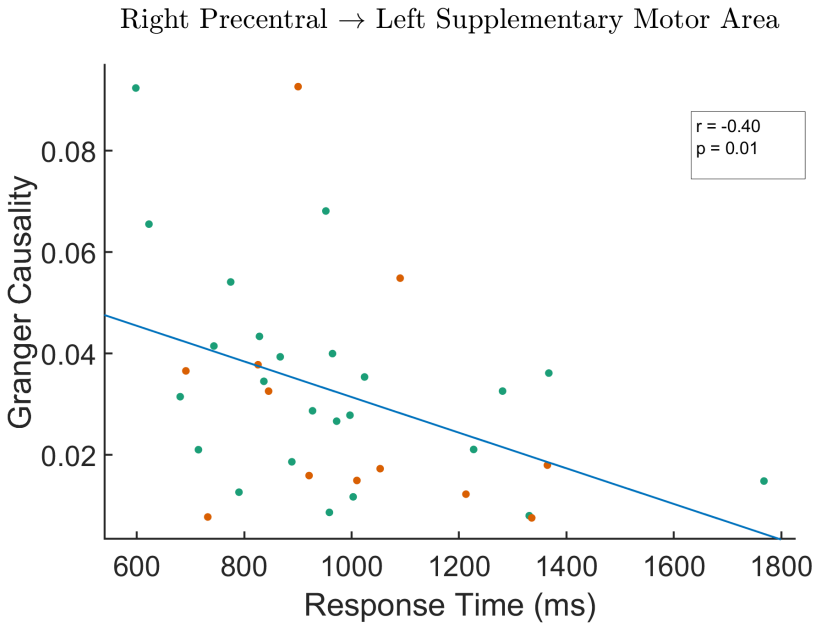

(b)

Figure 3.8 Scatter Plot for GC vs Response times to correlation neural mechanisms to behavioral performance. Figure 3.8a and 3.8b both were found to have moderate correlations that were significant $p < 0.05$.

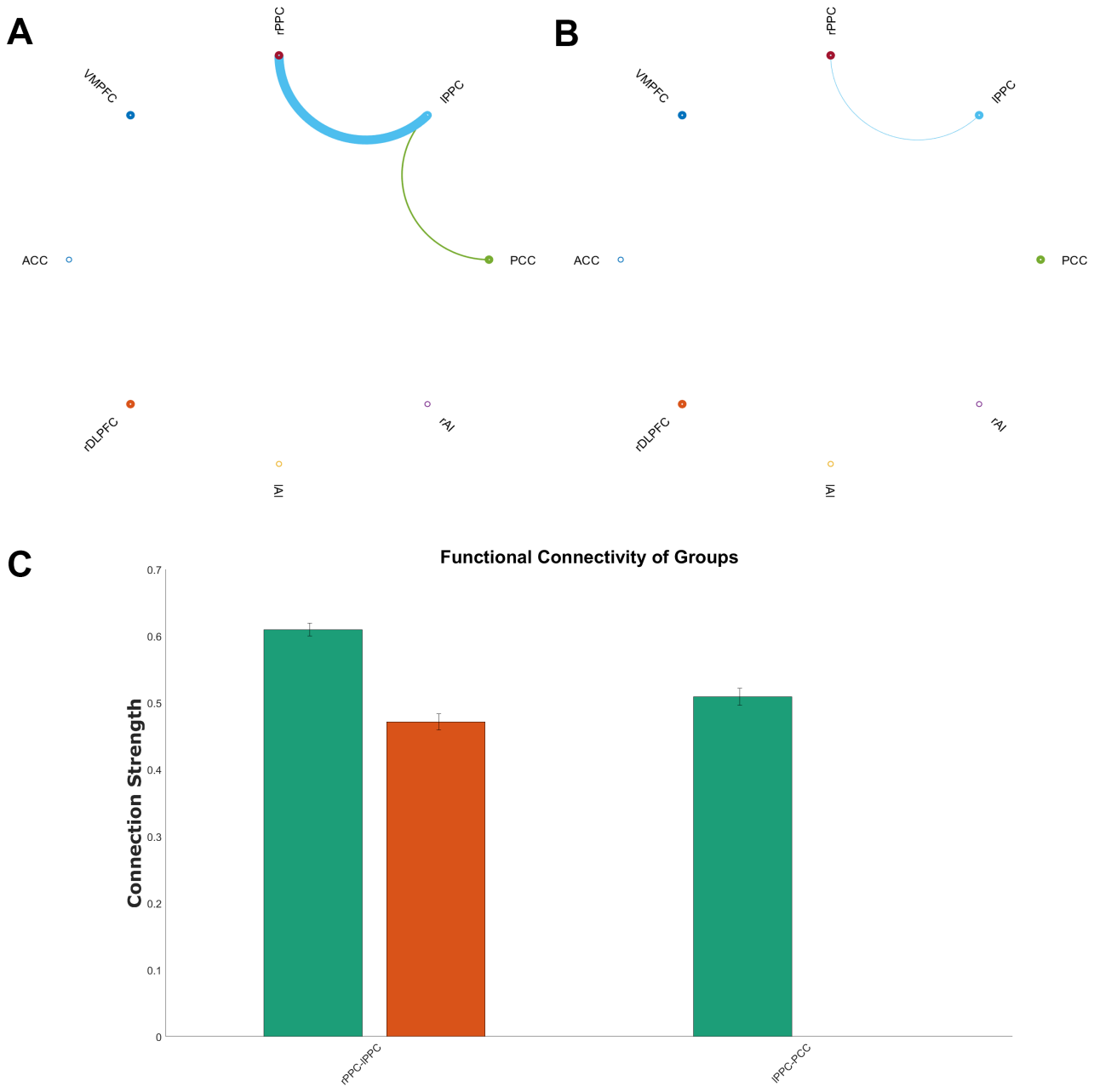

Figure 3.9 Significant Functional Connections. Line thickness indicates strength of connection, thicker line = higher connectivity and vice versa. A: Significant connections for VGP. B: Significant connections for NVGP. C: Comparison between significant connections in both groups, dark green for VGP and dark orange for NVGP

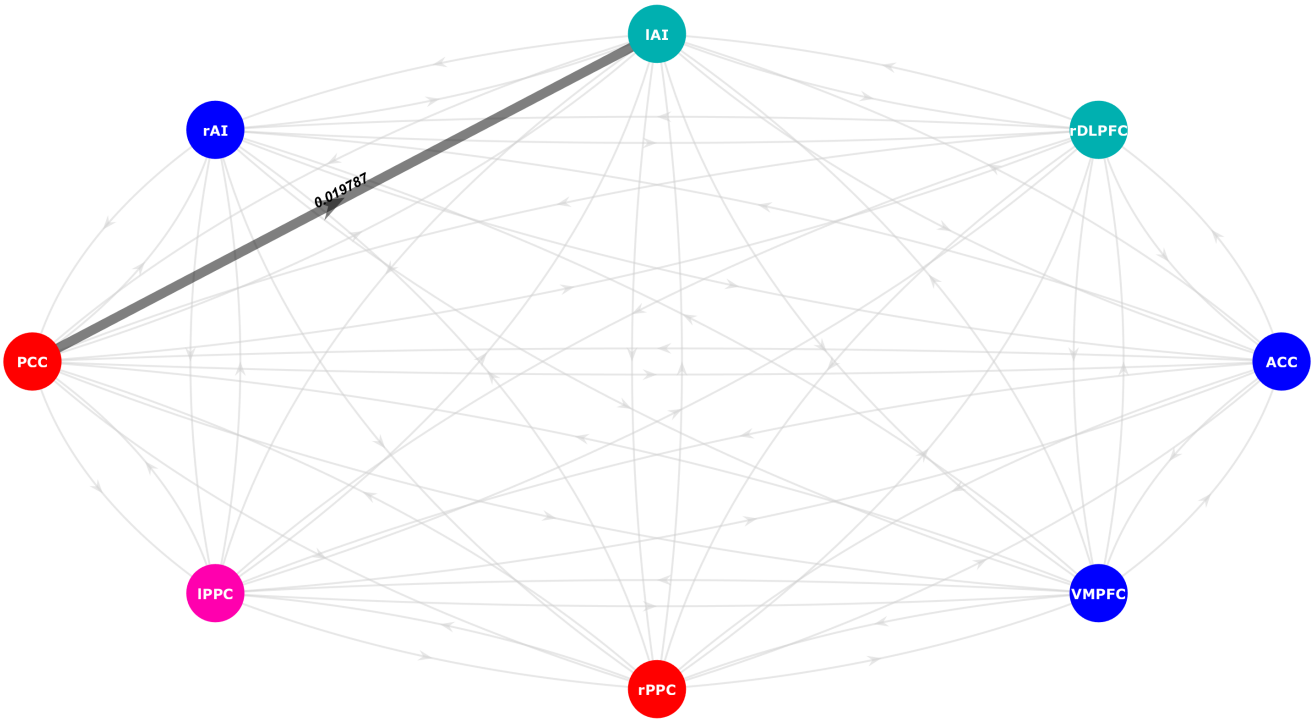

Figure 3.10 Significant directed Functional connectivity higher in VGP for CEN-DMN-SN network interactions. The corresponding GC value is displayed along the line.

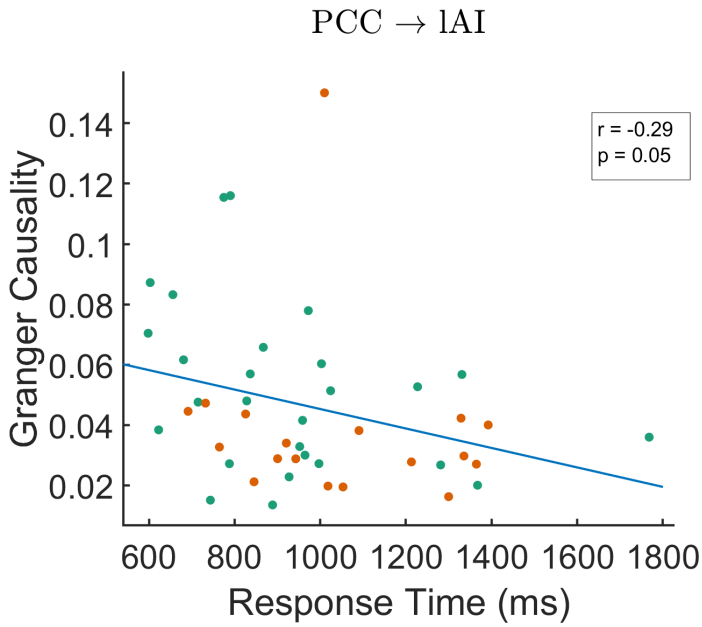

(a)

Figure 3.11 Scatter plot for PCC to left aI GC vs response times to correlation neural mechanisms to behavioral performance. Figure 3.11a was found to have moderate correlations that were significant $p < 0.05$.

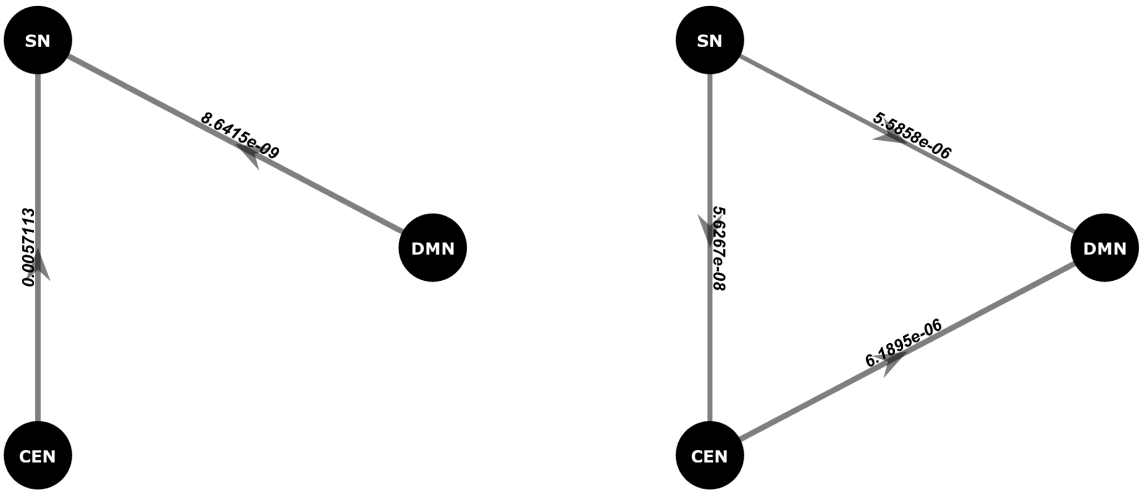

(a) (b)

Figure 3.12 Significant functional connections higher in VGP and NVGP for CEN-DMN-SN network interactions. Figure 3.12a and 3.12b correspond to VGP and NVGP, respectively.

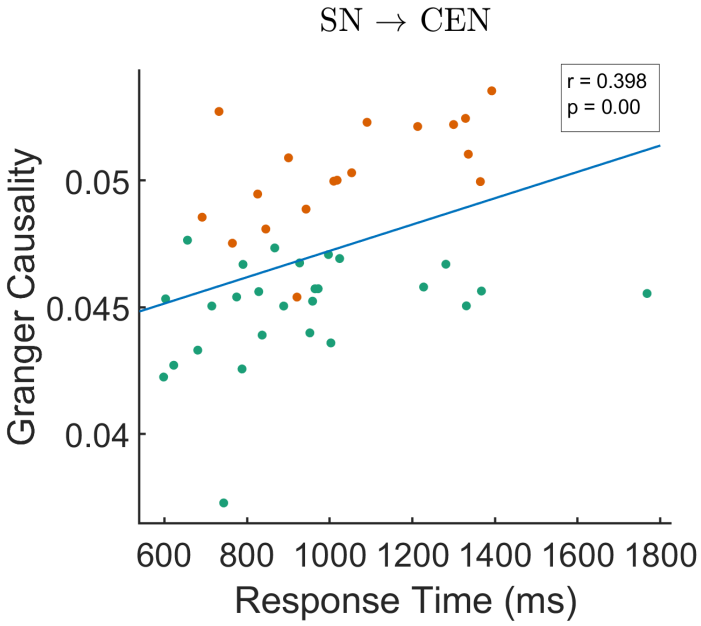

(a)

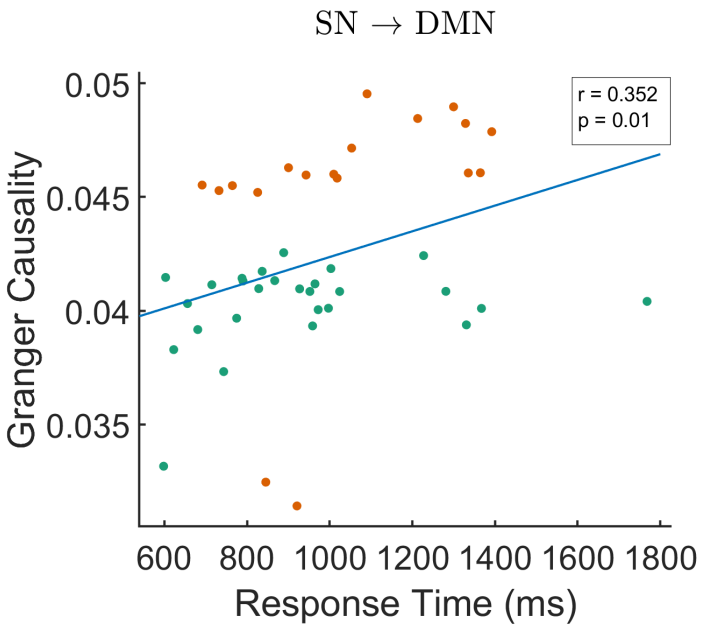

(b)

Figure 3.13 Scatter plot for GC vs response times to correlation neural mechanisms to behavioral performance. Figure 3.13a shows SN to CEN and 3.13b shows SN to DMN and both were found to have moderate correlations that were significant $p < 0.05$.

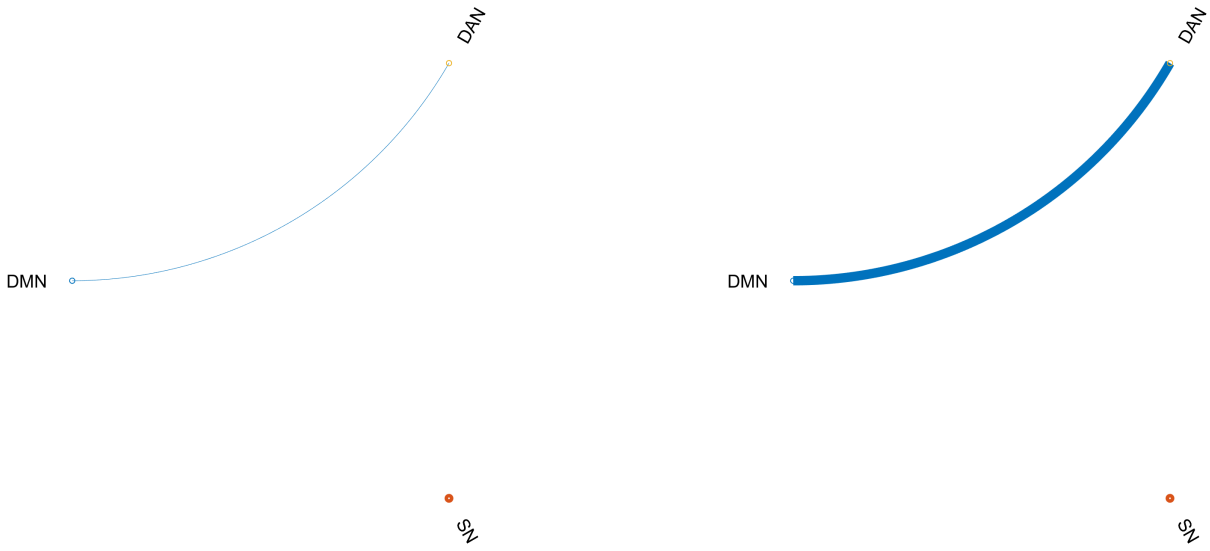

(a) (b)

Figure 3.14 Significant functional connections higher in NVGP for DAN-DMN-SN network interactions. Figure 3.14a and 3.14b correspond to VGP and NVGP, respectively.

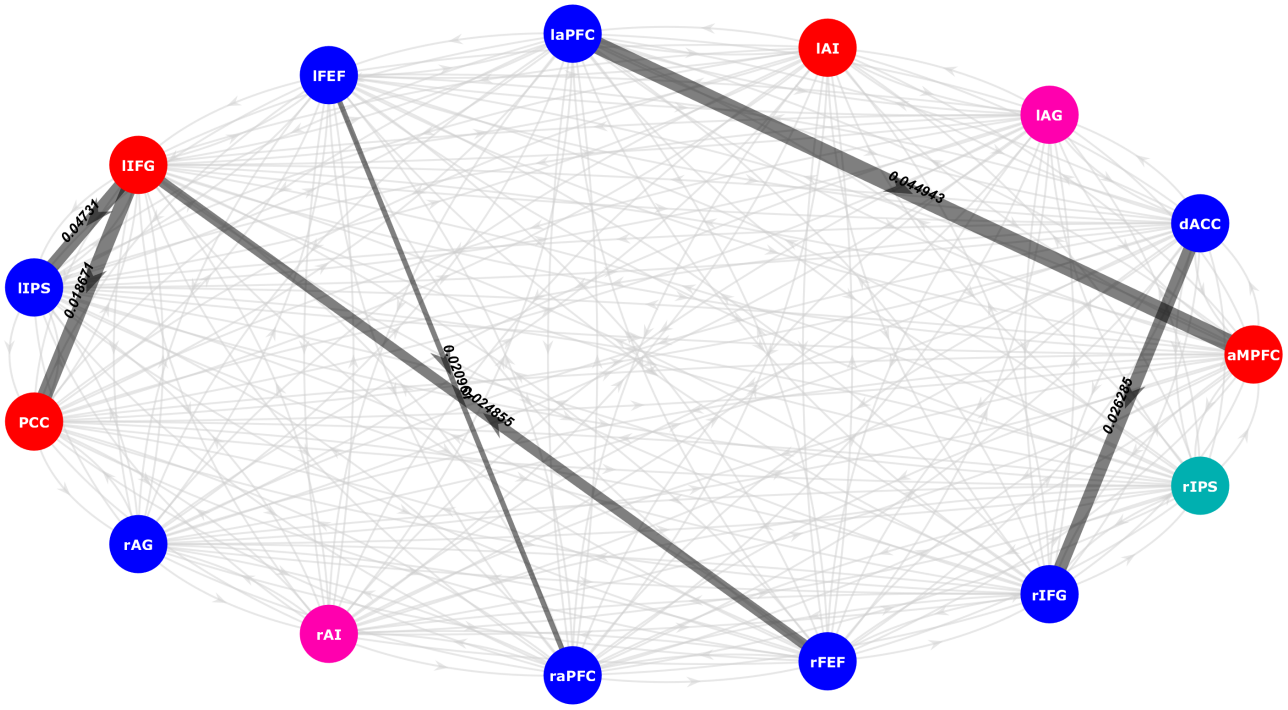

Figure 3.15 Significant directed functional connections higher in NVGP for DAN-DMN-SN network interactions. The corresponding GC value is displayed along the line.

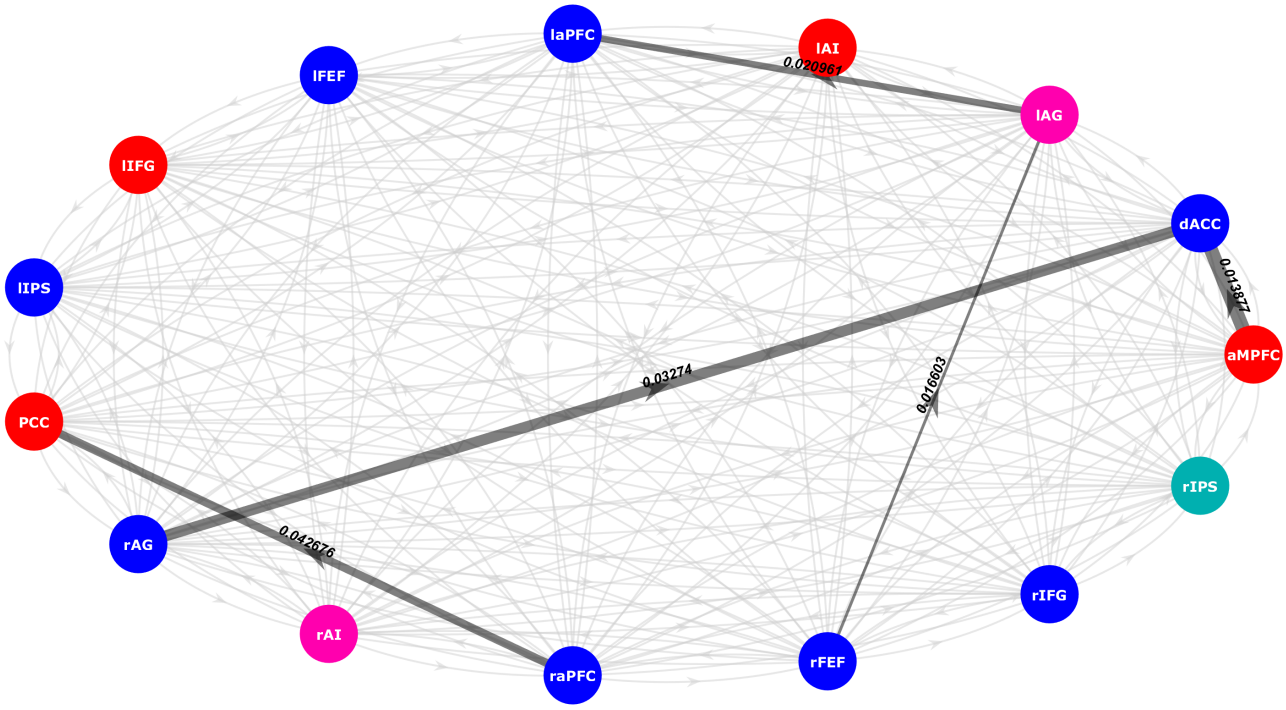

Figure 3.16 Significant directed functional connections higher in VGP for DAN-DMN-SN network interactions. The corresponding GC value is displayed along the line.

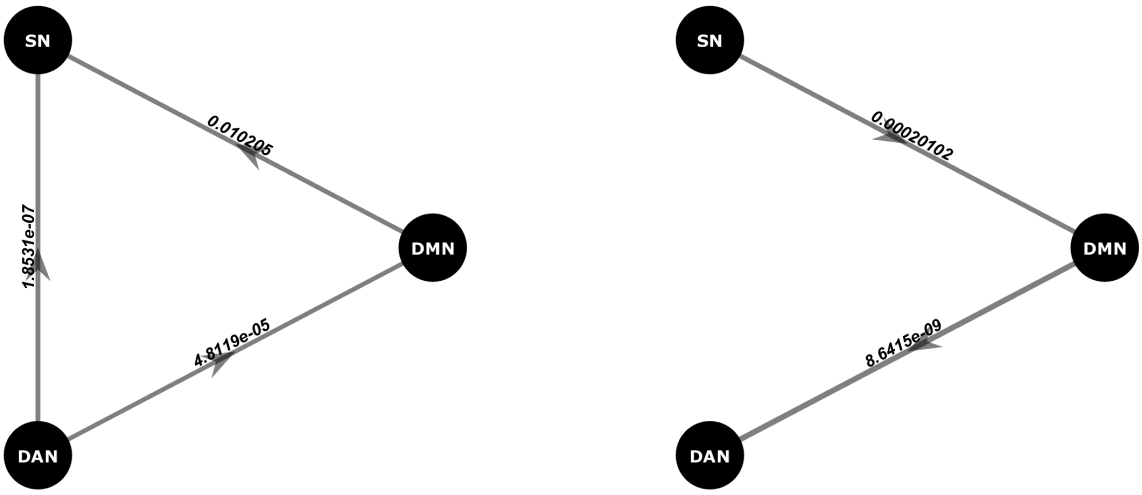

(a) (b)

Figure 3.17 Significant functional connections higher in VGP and NVGP for DAN-DMN-SN network interactions. Figure 3.17a and 3.17b correspond to VGP and NVGP, respectively.

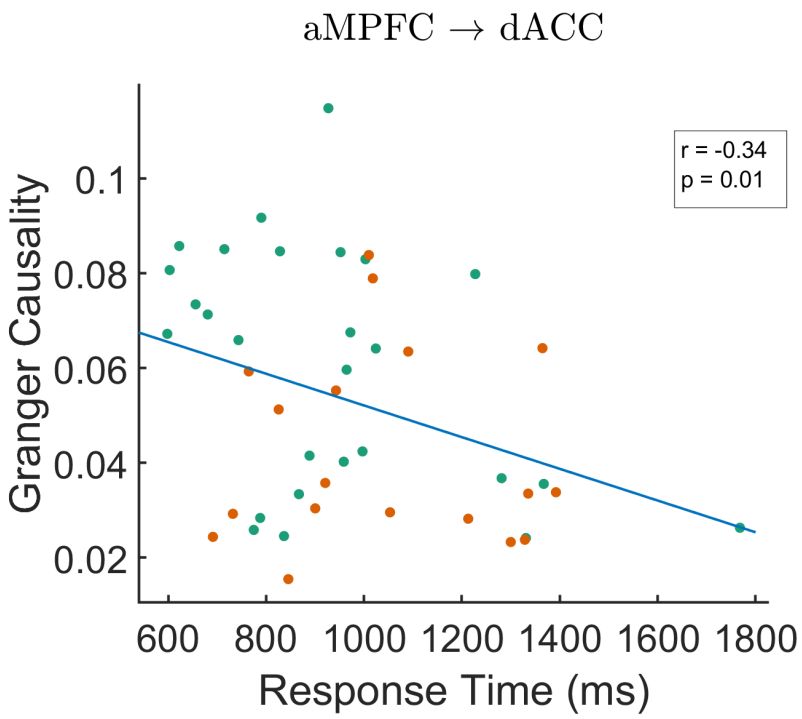

Figure 3.18 Scatter plot for aMPFC to dACC GC vs response times to correlation neural mechanisms to behavioral performance.

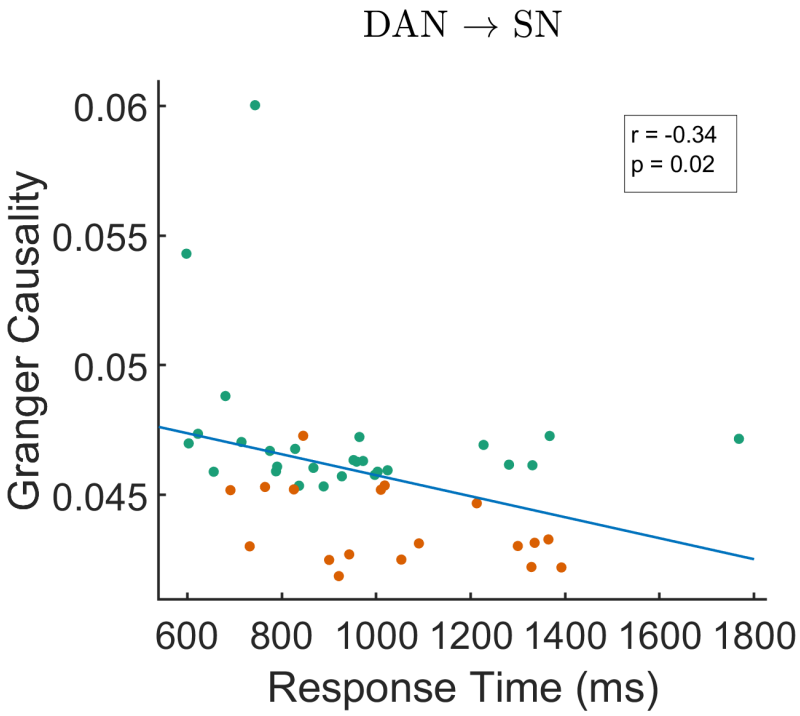

Figure 3.19 Scatter plot for DAN to SN GC vs response times to correlation neural mechanisms to behavioral performance.

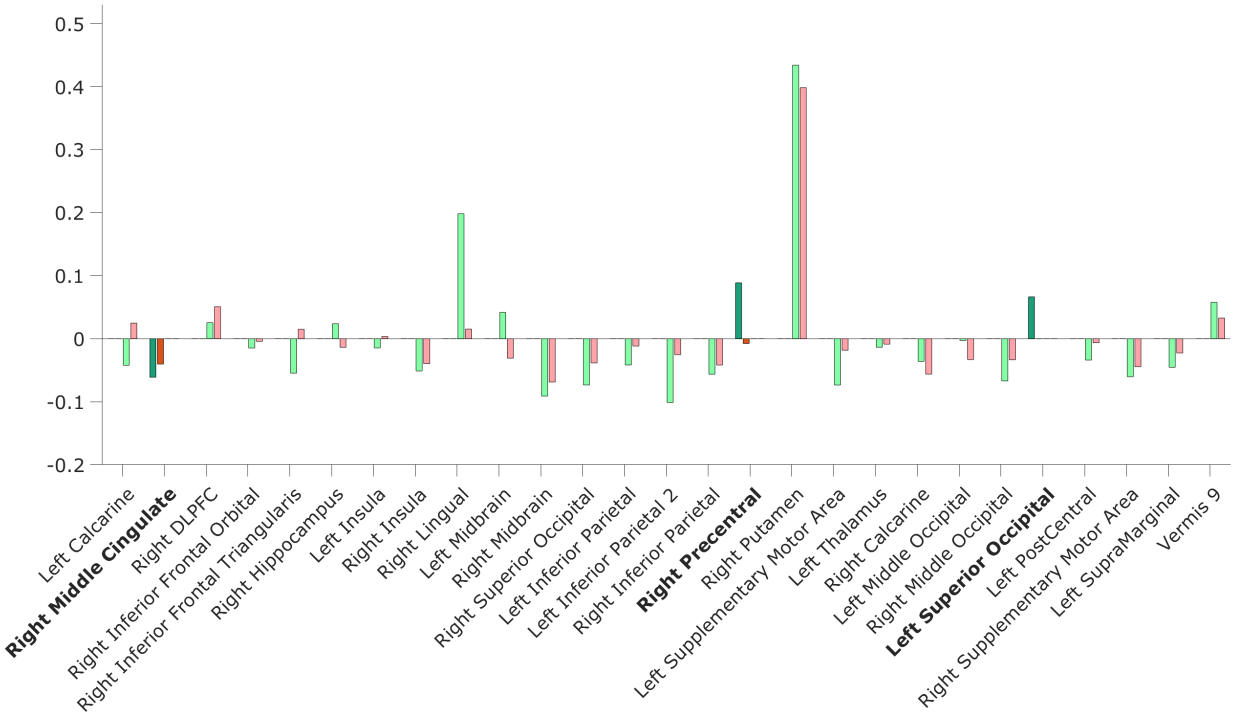

Figure 3.20 Netflow is shown by positive and negative Y bars for sink and source behavior, respectively. ROI labels in bold are the regions with significant group differences at $p < 0.05$.

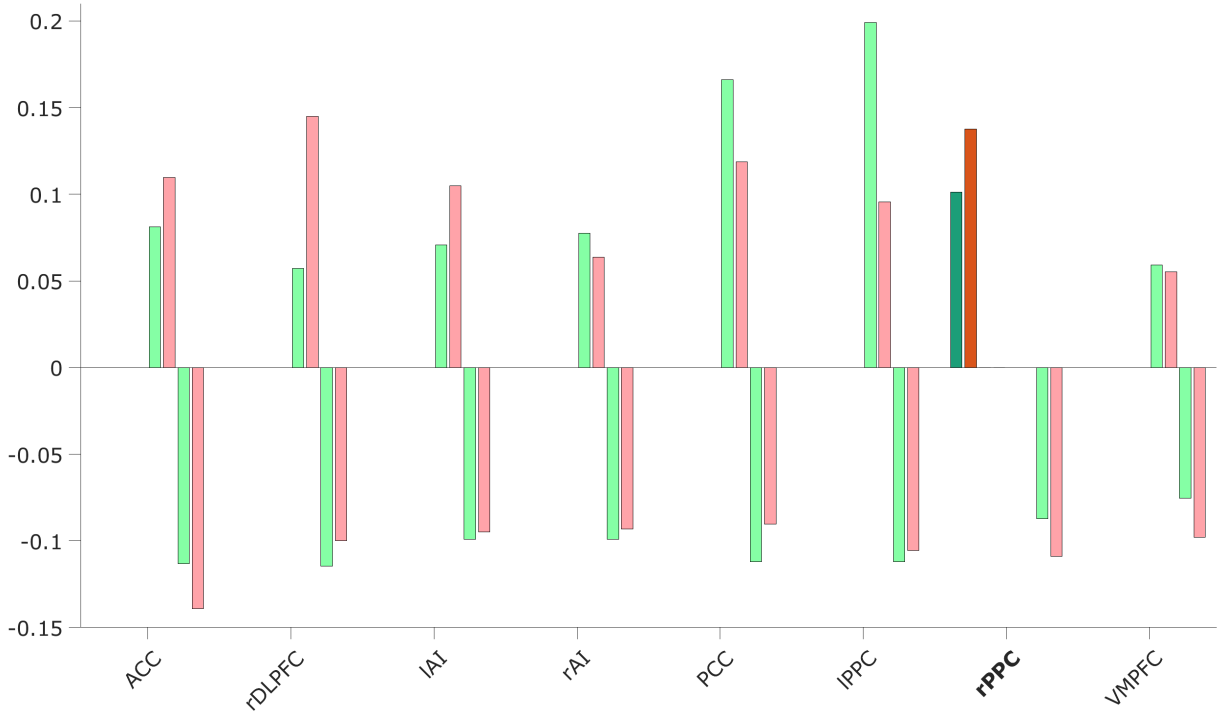

Figure 3.21 Inflow and Outflow are shown by positive and negative Y bars, respectively. ROI labels in bold are the regions with significant group differences at $p < 0.05$.

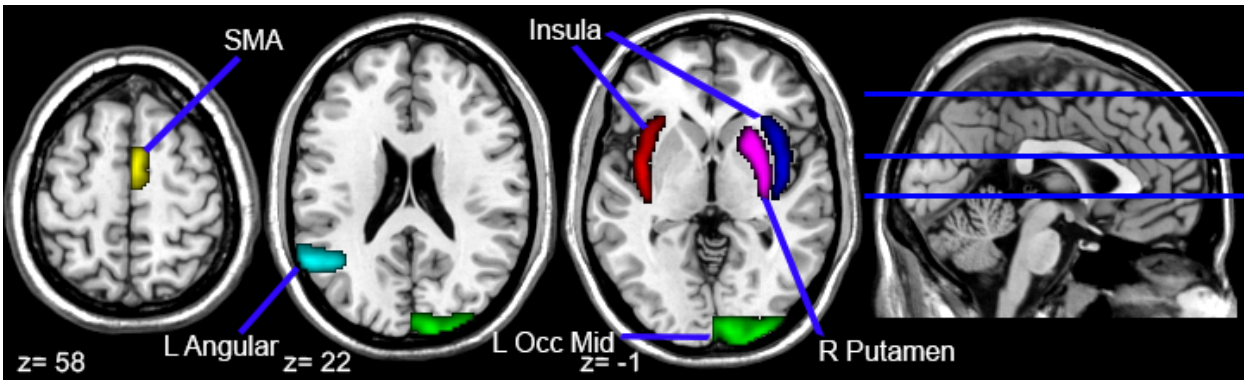

Figure 3.22 VBM regions found to have significant differences between groups. ROI masks taken from Harvard-Oxford cortical and subcortical structural atlases (Desikan et al. (2006))

CHAPTER 4
DISCUSSION & CONCLUSION

4.1 Discussion

This neuroimaging study investigated the change in decision-making abilities due to video game playing and the underlying brain mechanisms for these changes. These mechanisms involved the integration of information across multiple sub-processes including sensation, perception, and action (Siegel et al. (2011), Siegel et al. (2015)) as illustrated in figure 4.1. We compared VGP and NVGP for their behavioral and brain responses. VGP had increased decision accuracy and decision time in overall performance for MD left-right discrimination task. There were significant differences in both brain activity and connectivity. These results were consistent with both our predictions and previous studies (Basak et al. (2008), Green & Bavelier (2007), Green & Bavelier (2015), Li et al. (2009), Oei & Patterson (2014), Wu & Spence (2013)).

4.1.1 Task Related Regional Brain Activity

First, looking at the brain activations, we found that VGP had significantly higher percent signal change from baseline activations, specifically in left MOG, SMA, V9, right LING, left IPL, MB, and right PUT. These regions are known for visual processing (Binkofski et al. (2016), Galetta (2014), Lueck et al. (1989), Renier et al. (2010), Ramanoel et al. (2018), Zeki et al. (1991)), motor planning (Cunnington et al. (1996), Lanciego et al. (2012), Makoshi et al. (2011)), and visuomotor coordination (Caminero & Cascella (2020), Glickstein et al. (1994)). This could indicate that VGP utilize those regions more to be able to visually

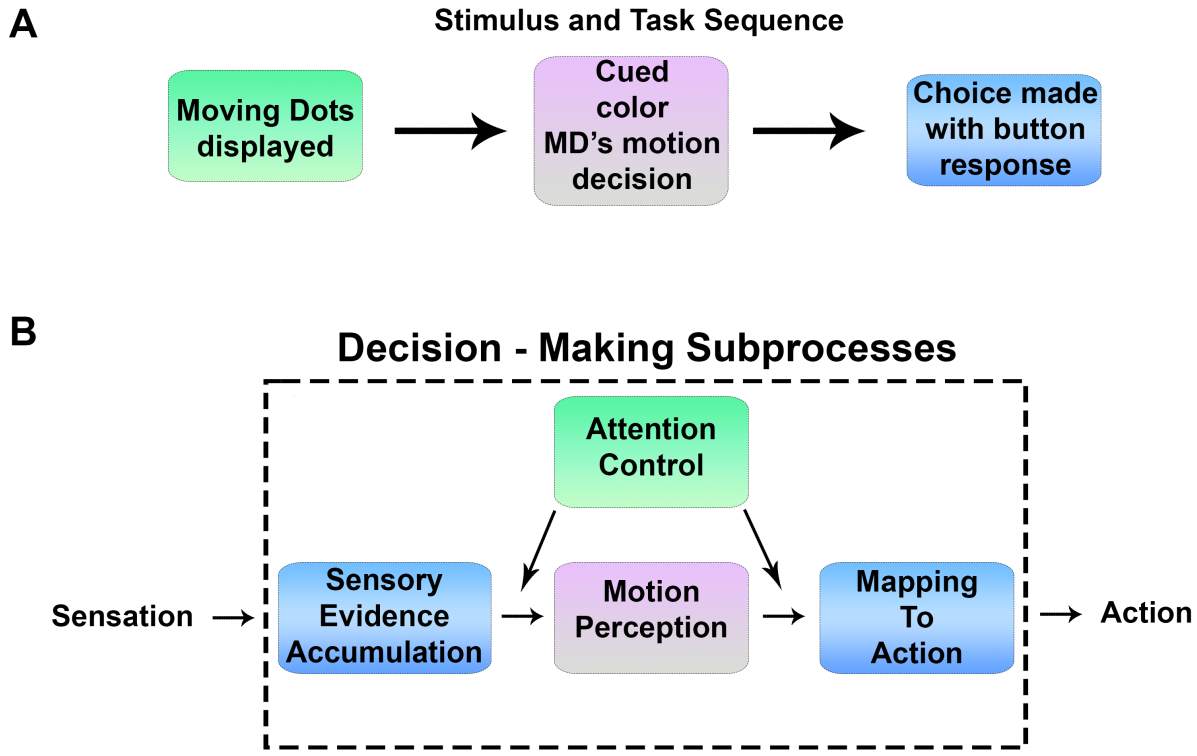

Figure 4.1 Sensorimotor Decision-Making Tasks and Subprocesses. Sensorimotor decision-making requires the processing and integration of information through multiple subprocesses A. Stimulus and Task sequence B. A breakdown of the decision-making process into its subprocesses.

process and react to the stimulus faster. Interestingly, NVGP showed higher percent signal change than VGP in the left IFT for higher speed tasks. This region has been shown to inhibit motor responses while still processing information (Molnar-Szakacs et al. (2004)). This could mean that NVGP have a higher inhibition to their motor areas, causing slower responses.

Likewise, examining net activity flow from each ROI, we found that there were significant group differences in motor, right MCC and right PreCG, and a visual region, left SOG. Although MCC acts as a sink region for both groups, VGP showed an increased inflow from

all other regions. Differences in the amount of information flow and behavior were seen for PreCG and SOG. For VGP, PreCG and SOG acted as a source region, while for NVGP, they acted as a sink and neutral region, respectively. An increase in outflow from SOG shows that VGP transmit more information after visual processing. MCC has been shown to correspond to selective attention and response timing for timed decisions (Vogt (2016)). Here, an increase in information inflow for VGP could indicate that VGP utilize more task-relevant information in motor response timing. PreCG is responsible for motor execution, so it would be expected to act primarily as a sink; however, VGP utilized it more as a source. This may indicate some feedback from the PreCG that VGP utilize more than NVGP.

Next, we wanted to see how video game playing had modulated brain connectivity for decision-making tasks. Six connections were elevated in VGP compared to NVGP; out of the six, only three were seen in NVGP. VGP showed higher correlations for all connections. Of the three connections that both groups had, right SOG - left Calcarine (CAL), left MOG-left CAL, and left SOG-right IPL correspond to connections between visual processing ROI (Binkofski et al. (2016), Galetta (2014), Russo et al. (2001), Macaluso et al. (2003)). The remaining connections, V9-right IPL, left MOG-left THA, and left THA-right SOG, were only present in VGP. Both V9 and right IPL have been shown to play roles in visuomotor coordination (Binkofski et al. (2016), Guell & Schmahmann (2019), Ramanoel et al. (2018)). A higher connection between these two could suggest being able to coordinate responses faster and more accurately from processing the visual stimulus.

Characterizing directed functional connectivity with CGC, we found four elevated connections in VGP. Two of these connections, right IPL to left MOG and right PUT to left CAL,

could be benefiting the subprocess of mapping to action for sensorimotor decision-making. Right IPL plays a role in spatial coding (Binkofski et al. (2016)), and left MOG which plays a role spatial (Renier et al. (2010)), color and motion processing (Galetta (2014)). Increased connectivity between these two regions indicates increased spatial resolution of the task dedicated space. We also see increased influence of the right LING to right MCC. The Lingual Gyrus has been indicated as being the Human V4, which plays a role in color perception (Lueck et al. (1989), Zeki et al. (1991), Zeki & Bartels (1999)), while MCC plays a part in motor planning (Vogt (2016)). Increases in this connection could help motor planning responses to the cued color dots. Lastly, we saw higher connectivity from right PreCG to left THA. PreCG is the primary motor area responsible for motor execution, and THA is a sensory hub that relays signals between cortices. This connection could potentially be a feedback loop after decision execution.

The second set of connections we examined were those including DLPFC. DLPFC has been shown to play a role in the decision-making processes (Donahue & Lee (2015), Heekeren et al. (2006), Philiastides et al. (2011)) and as well as having increased activity in VGP (Granek et al. (2010)), so we wanted to look closer at how video game playing modulated its connections. We see that it increases the DLPFC's influence on visual areas right MOG and right CAL as well as right Inferior Frontal pars orbitalis (IFO), which plays a role in the semantic processing of words (Belyk et al. (2017)). Increases in these connections show top-down attention control, which agrees with observations made by Green & Bavelier (2015) and Wu & Spence (2013). The increased connectivity with IFO could indicate better cue processing to keep track of the prompted color.

4.1.2 Central Executive - Default Mode - Salience Networks

After looking at the regions with brain activations, we focused on network-to-network connectivity (considering each Network as a node) to examine interactions. The first set of networks were CEN, DMN, and SN. Chand & Dhamala (2016) showed that the SN exerts a causal control over DMN and CEN in decision-making. In our results, we see that this behavior gets increased in NVGP compared to VGP. In contrast, we found that in VGP, causal control of SN was lower, and instead, DMN and CEN had increased causal influence over SN. This could potentially mean that control of SN instead of SN control is vital for increased decision-making performance.

Node-to-node connectivity among all nodes of all networks from undirected and directed FC analyses showed increased influence from PCC to left aI and PCC to PPC. PCC is part of the DMN and plays a role in improving behavioral performance by controlling attention focus (Leech & Sharp (2013)). The anterior Insula is part of SN and is responsible for engaging attention and awareness of salient stimuli (Menon & Uddin (2010)). Therefore, increased influence of PCC on left aI could mean increased attention control towards task-relevant stimuli. Comparing this connection to RT, we see as this connection becomes stronger performance increase, via response time decrease, supporting this claim. These results correlate with (Wu & Spence (2013)) that showed VGP had increased attention control with increased performance.

Lastly, from undirected FC and information flow, VGP showed increased FC and information outflow from PPC. PPC is responsible for proper object-oriented actions (Jeannerod

(2001)) and spatial attention (Groh & Werner-reiss (2002)). This is consistent with results for goal-directed actions.

4.1.3 Dorsal Attention-Default Mode-Salience Networks

Zhou et al. (2017) examined attention switching from rest to task-active state in young adults, looking at the network interactions between DAN, DMN, and SN, showing that SN exerts causal influence over DAN and DMN. We examined these network interactions in our participants who were in the same age range. NVGP exhibited this neural activity with increased causal influence over the DMN, but VGP showed increased influence over SN from DAN and DMN. Our correlation results from GC vs. RT showed that RT increased with GC from DAN to SN decreasing. Although SN may coordinate the switch from rest to executive control, influence to SN may be required for more effective switching when in a task-based environment. We see in VGP an increase in DAN's causal influence to both SN and DMN, indicated visual attention-driven mode switching from rest to task-active state. This could allow for the increased response time for VGP if they are able to become task-focused more quickly.

4.2 Conclusions

In this dissertation, we have looked at the brain mechanisms for enhanced sensorimotor decision-making for VGP compared to NVGP. We examined their differences at both the brain regional and network-level for undirected and directed functional connectivity as well as structural changes. We showed that VGP outperform NVGP on a decision-making

task overall for accuracy but consistently demonstrated a significantly higher response time. From our activation-based ROI analyses, we see that there were significant differences in regions involved with both visual processing and motor movement/planning. We also saw an increased influence from DLPFC to visual information-processing regions. At the network level, we saw that VGP increased influence to the SN from all other networks. This also correlated with the response time.

To summarize, video game playing alters somatosensory-parietal network dynamics of the decision-making process, allowing them to respond more quickly and accurately. Our evidence supports that increased influence to the SN causes increased decision-making performance. We theorize that this means that VGP are able to better control what object they deem as important and control their attention to focus more solely on that object, thus resolving it more quickly for the response.

4.3 Outlook for Future Studies

The next step would be to examine white matter tracts between these networks to correlate the functional connectivity results. There is much left to be examined for functional connectivity between VGP and NVGP; whole brain and condition-specific analyses. For this study, we differentiated the type of gamer based on the game genre they primarily played for the required amount per week but were unable to examine the differences amongst video game players in this study. Future studies should see if the effects seen here in this study still stand if the VGP are divided into groups based on their respective gaming type. Functional MRI is limited by its time resolution capabilities and indirect measure of brain activity.

Future studies would benefit by using electroencephalography (EEG) to expand on these results for better time resolution of decision-making sub-processes.

REFERENCES

Andersson, M. J., & Smith, S. 2007, Non-linear registration, aka Spatial normalisation

Anguera, J. A. et al. 2013, Nature, 501, 97

Basak, C., Boot, W. R., Voss, M. W., & Kramer, A. F. 2008, Psychology and Aging, 23, 765

Belyk, M., Brown, S., Lim, J., & Kotz, S. A. 2017, NeuroImage, 156, 240

Binkofski, F. C., Klann, J., & Caspers, S. 2016, in Neurobiology of Language, ed. G. Hickok & S. L. Small (San Diego: Academic Press), 35–47

Brett, M., Anton, J., Valabregue, R., & Poline, J. 2002, Human Brain Mapping Conference, 16, 497

Brovelli, A., Ding, M., Ledberg, A., Chen, Y., Nakamura, R., & Bressler, S. L. 2004, Proceedings of the National Academy of Sciences, 101, 9849

Caminero, F., & Cascella, M. 2020, Neuroanatomy, Mesencephalon Midbrain (Treasure Island (FL): StatPearls Publishing), 31855353[pmid]

Chand, G. B., & Dhamala, M. 2016, Brain Connectivity, 6, 249

Cox, R. W. 1996, Computers and Biomedical Research, 29, 162

Cox, R. W., & Hyde, J. S. 1997, NMR in Biomedicine, 10, 171

Cunnington, R., Iansek, R., Bradshaw, J., & Phillips, J. 1996, Experimental Brain Research, 111

Desikan, R. S. et al. 2006, NeuroImage, 31, 968

Dhamala, M., Rangarajan, G., & Ding, M. 2008, NeuroImage, 41, 354

Donahue, C. H., & Lee, D. 2015, Nature Neuroscience, 18, 295

Douaud, G. et al. 2007, Brain, 130, 2375

Friston, K. J. 2010, Statistical parametric mapping: The analysis of functional brain images (Elsevier AP)

Galetta, S. 2014, in Encyclopedia of the Neurological Sciences (Elsevier), 626–632

Glickstein, M., Gerrits, N., Kralj-Hans, I., Mercier, B., Stein, J., & Voogd, J. 1994, The Journal of Comparative Neurology, 349, 51

Glover, G. H. 2011, Neurosurgery Clinics of North America, 22, 133

Gong, D. et al. 2016, Neural Plasticity, 2016, 1

Good, C. D., Johnsrude, I. S., Ashburner, J., Henson, R. N., Friston, K. J., & Frackowiak, R. S. 2001, NeuroImage, 14, 21

Granek, J. A., Gorbet, D. J., & Sergio, L. E. 2010, Cortex, 46, 1165

Green, C., & Bavelier, D. 2007, Psychological Science, 18, 88

Green, C. S., & Bavelier, D. 2003, Nature, 423, 534

——. 2015, Current Opinion in Behavioral Sciences, 4, 103

Groh, J. M., & Werner-reiss, U. 2002, in Encyclopedia of the Human Brain (Elsevier), 739–752

Guell, X., & Schmahmann, J. 2019, The Cerebellum, 19, 1

Han, D. H., Lyoo, I. K., & Renshaw, P. F. 2012, Journal of Psychiatric Research, 46, 507

Heekeren, H. R., Marrett, S., Ruff, D. A., Bandettini, P. A., & Ungerleider, L. G. 2006, Proceedings of the National Academy of Sciences, 103, 10023

Jeannerod, M. 2001, in International Encyclopedia of the Social & Behavioral Sciences (Elsevier), 16224–16228

Lanciego, J. L., Luquin, N., & Obeso, J. A. 2012, Cold Spring Harbor Perspectives in Medicine, 2, a009621

Leech, R., & Sharp, D. J. 2013, Brain, 137, 12

Li, R., Polat, U., Makous, W., & Bavelier, D. 2009, Nature Neuroscience, 12, 549

Lueck, C. J. et al. 1989, Nature, 340, 386

Lynch, J., Aughwane, P., & Hammond, T. M. 2010, Journal of Surgical Education, 67, 184

Macaluso, E., Eimer, M., Frith, C. D., & Driver, J. 2003, Experimental Brain Research, 149, 62

Makoshi, Z., Kroliczak, G., & van Donkelaar, P. 2011, Journal of Motor Behavior, 43, 303

Maldjian, J. A., Laurienti, P. J., Kraft, R. A., & Burdette, J. H. 2003, NeuroImage, 19, 1233

Menon, V., & Uddin, L. Q. 2010, Brain Structure and Function, 214, 655

Molnar-Szakacs, I., Iacoboni, M., Koski, L., & Mazziotta, J. C. 2004, Cerebral Cortex, 15, 986

Momi, D., Smeralda, C. L., Lorenzo, G. D., Neri, F., Rossi, S., Rossi, A., & Santarnecchi, E. 2020, Brain Imaging and Behavior, 15, 1518

Oei, A. C., & Patterson, M. D. 2014, Computers in Human Behavior, 37, 216

Palaus, M., Marron, E. M., Viejo-Sobera, R., & Redolar-Ripoll, D. 2017, Frontiers in Human Neuroscience, 11

Peirce, J., Gray, J. R., Simpson, S., MacAskill, M., Höchenberger, R., Sogo, H., Kastman, E., & Lindeløv, J. K. 2019, Behavior Research Methods, 51, 195

Philiastides, M., Auksztulewicz, R., Heekeren, H., & Blankenburg, F. 2011, Current Biology, 21, 980

Ramanoel, S., York, E., & Habas, C. 2018, Cerebellum & Ataxias, 5, 9

Renier, L. A., Anurova, I., Volder, A. G. D., Carlson, S., VanMeter, J., & Rauschecker, J. P. 2010, Neuron, 68, 138

Reynaldo, C., Christian, R., Hosea, H., & Gunawan, A. A. S. 2021, Procedia Computer Science, 179, 211, 5th International Conference on Computer Science and Computational Intelligence 2020

Richlan, F., Schubert, J., Mayer, R., Hutzler, F., & Kronbichler, M. 2017, Brain and Behavior, 8, e00877

Rosser, J. C. 2007, Archives of Surgery, 142, 181

Russo, F. D., Martínez, A., Sereno, M. I., Pitzalis, S., & Hillyard, S. A. 2001, Human Brain Mapping, 15, 95

Siegel, M., Buschman, T. J., & Miller, E. K. 2015, Science, 348, 1352

Siegel, M., Engel, A. K., & Donner, T. H. 2011, Frontiers in Human Neuroscience, 5

Smith, S. M. et al. 2004, NeuroImage, 23, S208

Sridharan, D., Levitin, D. J., & Menon, V. 2008, Proceedings of the National Academy of Sciences, 105, 12569

Tanaka, S. et al. 2013, PLOS ONE, 8, 1

Vogt, B. A. 2016, Journal of Chemical Neuroanatomy, 74, 28

Wen, X., Rangarajan, G., & Ding, M. 2013, Philosophical Transactions of the Royal Society A: Mathematical, Physical and Engineering Sciences, 371, 20110610

Wu, S., & Spence, I. 2013, Attention, Perception, & Psychophysics, 75, 673

Zeki, S., & Bartels, A. 1999, Philosophical Transactions of the Royal Society of London.

Series B: Biological Sciences, 354, 1371

Zeki, S., Watson, J. D., Lueck, C. J., Friston, K. J., Kennard, C., & Frackowiak, R. S. 1991, The Journal of neuroscience : the official journal of the Society for Neuroscience, 11, 641, 2002358[pmid]

Zhou, Y., Friston, K. J., Zeidman, P., Chen, J., Li, S., & Razi, A. 2017, Cerebral Cortex, 28, 726

APPENDIX A

SUPPLEMENTARY FIGURES & PLOTS

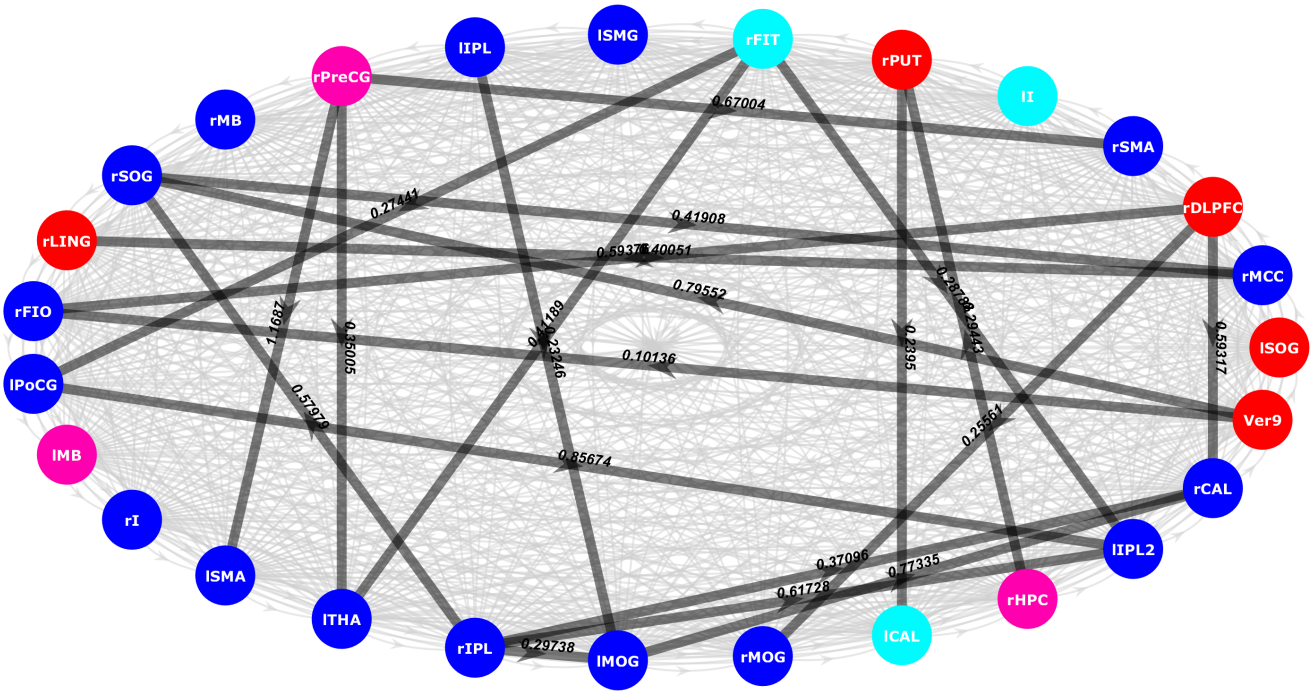

Figure A.1 All significant functional connections that were higher in VGP. Corresponding GC values are displayed along the line. Color of the nodes corresponds to source or sink behavior of the region. Blue corresponds to sink behavior for both groups. Red corresponds to source behavior for both groups. Light blue corresponds to regions that were sink for VGP and source for NVGP. Pink corresponds to regions that were source for VGP and sink for NVGP.

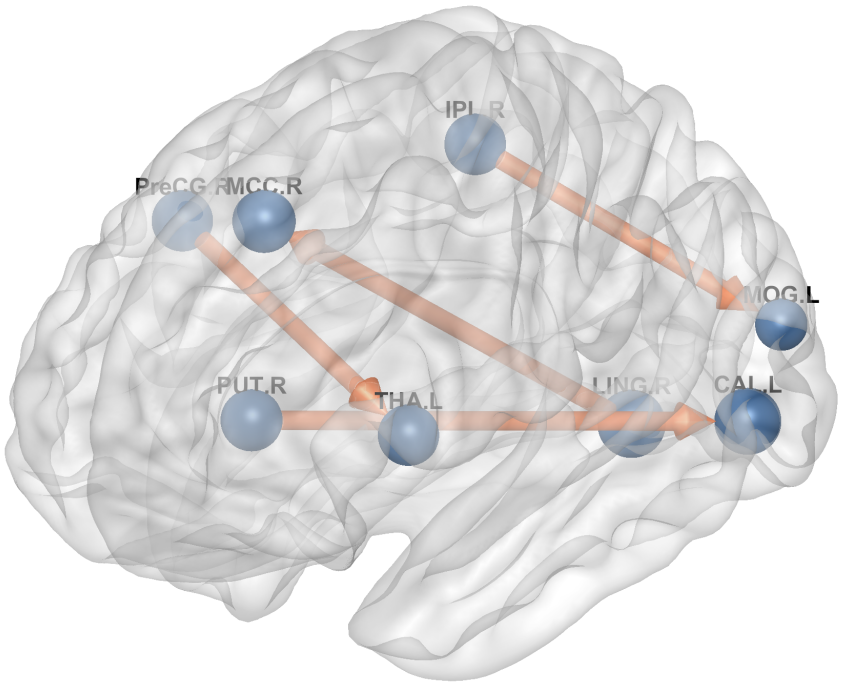

Figure A.2 Significant direct FC in VGP at significance $p < 0.01$.

APPENDIX B

SUPPLEMENTARY TABLES

Table B.1 Functional Connectivity correlation values

Connection	VG	NVG	p
Left Calcarine - Right Superior Occipital	0.8415	0.7671	0.0386
Left Calcarine - Left Middle Occipital	0.7858	0.6961	0.0384
Right Superior Occipital - Left Thalamus	0.4008	0	0.0442
Right Inferior Parietal - Left Superior Occipital	0.7143	0.5923	0.0466
Right Inferior Parietal - Vermis 9	0.5402	0	0.0228
Left Thalamus - Left Middle Occipital	0.4427	0	0.0364

Supplementary Table for FC connections with p value for Activation Based ROI interactions

Table B.2 Functional Connectivity correlation values for CEN-SN-DMN Network

Connection	VG	NVG	p
PCC - lPPC	0.5092	0	0.0214
lPPC - rPPC	0.6098	0.4715	0.0110

Supplementary Table for FC connections with p value for CEN-DMN-SN ROI interactions

Table B.3 Region of Interest Netflow for Activation Based ROI

Contrast	Region of Interest	VG	NVG
Task-Rest	Left Calcarine	Sink	Source
	Right Middle Cingulate	Sink	Sink
	Right Inferior Frontal Orbital	Sink	Sink
	Right Inferior Frontal Triangularis	Sink	Source
	Right Hippocampus	Source	Sink
	Left Insula	Sink	Source
	Right Insula	Sink	Sink
	Right Lingual	Source	Source
	Left Midbrain	Source	Sink
	Right Midbrain	Sink	Sink
	Right Superior Occipital	Sink	Sink
	Left Inferior Parietal	Sink	Sink
	Left Inferior Parietal 2	Sink	Sink
	Right Inferior Parietal	Sink	Sink
	Right Precentral	Source	Sink
	Right Putamen	Source	Source
	Left Supplementary Motor Area	Sink	Sink
	Left Thalamus	Sink	Sink
Motion- No-Motion	Right Calcarine	Sink	Sink
	Left Middle Occipital	Sink	Sink
	Right Middle Occipital	Sink	Sink
	Left Superior Occipital	Source	Source
	Left PostCentral	Sink	Sink
	Right Supplementary Motor Area	Sink	Sink
	Left SupraMarginal	Sink	Sink
	Vermis 9	Source	Source

Net behavior of regions for each group. Used for node color of GC connection figures.

Table B.4 Mann-Whitney U-test Results for Granger Causality

Connection	VG	NVG	p	Z
Left Inferior Parietal→Left Middle Occipital	0.0195	0.0143	0.0222	2.287
Left Middle Occipital→Right Calcarine	0.0288	0.0178	0.0405	2.0485
Left PostCentral→Left Inferior Parietal 2	0.023	0.0122	0.0139	2.4604
Left Thalamus→Right Inferior Frontal Triangularis	0.0179	0.0117	0.0263	2.222
Right DLPFC→Right Calcarine	0.0243	0.0151	0.0427	2.0269
Right DLPFC→Right Inferior Frontal Orbital	0.0226	0.0141	0.0327	2.1353
Right DLPFC→Right Middle Occipital	0.0253	0.0161	0.0473	1.9835
Right Hippocampus→Right Putamen	0.0184	0.0105	0.031	2.1569
Right Inferior Frontal Triangularis→Left Inferior Parietal 2	0.0261	0.0164	0.0498	1.9618
Right Inferior Frontal Triangularis-Left PostCentral	0.0193	0.0118	0.0263	2.222
Right Inferior Parietal→Left Inferior Parietal 2	0.0307	0.0156	0.0166	2.3954
Right Inferior Parietal→Left Middle Occipital	0.0226	0.0133	0.0084	2.6338
Right Inferior Parietal→Right Calcarine	0.0228	0.0167	0.0327	2.1353
Right Inferior Parietal→Right Superior Occipital	0.0241	0.0132	0.0131	2.4821
Right Lingual→Right Middle Cingulate	0.02	0.0117	0.0079	2.6555
Right Precentral→Left Supplementary Motor Area	0.0302	0.0199	0.0294	2.1786
Right Precentral→Left Thalamus	0.0189	0.0109	0.0084	2.6338
Right Precentral→Right Supplementary Motor Area	0.0237	0.0132	0.0346	2.1136
Right Putamen→Left Calcarine	0.0232	0.0125	0.0061	2.7422
Right Superior Occipital→Right Middle Cingulate	0.0233	0.0157	0.0139	2.4604
Vermis 9→Right Inferior Frontal Orbital	0.0184	0.0143	0.031	2.1569
Vermis 9→Right Superior Occipital	0.0305	0.018	0.021	2.3087

All directed connections higher in VGP for Decision-Making Tasks

APPENDIX C

DEFINITIONS - STATISTICS AND MATHEMATICAL MEASURES USED

A Mann-Whitney U Test

The Mann-Whitney U test (also known as Wilcoxon Rank Sum Test) is a nonparametric equivalent of the parametric t-test used to determine differences between groups. To calculate and determine significance, all values from each group are brought together to determine the value's rank. The ranks go from $1-N$, where N is the total number of points for both groups combined. If the same value appears multiple times, then they are first assigned randomly to ranks in order. For example, if 1 appears 3 times and is the lowest value, then the lowest 3 ranks (1,2, and 3) will randomly be assigned to each 1 value. After all, values have been assigned a rank; all repeated values have their rank adjusted to give all values the same rank. This is done by using the following equation:

$$r_{adj} = \frac{\sum_{i=1}^{j} r_j}{j} \tag{C.1}$$

where r_j are the initial ranks assigned to the values, j is the number of times the value is repeated, and r_adj is the adjusted rank for the value. Once all values have been assigned a rank, these ranks are summed together to get the group's total rank R. With the total rank, we then calculate the U statistic for each group as follows:

$$U_{G1} = n_{G1} \cdot n_{G2} + \frac{n_{G1}(n_{G1}+1)}{2} + R_{G1} \tag{C.2a}$$

$$U_{G2} = n_{G1} \cdot n_{G2} + \frac{n_{G2}(n_{G2}+1)}{2} + R_{G2} \tag{C.2b}$$

Since one of our groups is large than 20 participants, we must use an approximate normalization assumption and test for significance using a z-test. we calculated significance using the following equation:

$$z = \frac{U - \mu_U}{\sigma_U} \tag{C.3}$$

where U is the larger of the two Us calculated above, μ_U is the mean of U, and σ_U is the variance of U calculated using:

$$\mu_U = \frac{n_{G1} \cdot n_{G2}}{2} \tag{C.4a}$$

$$\sigma_U = \sqrt{\frac{n_{G1} n_{G2} (n_{G1} - n_{G2} + 1)}{12}} \tag{C.4b}$$

If $z > 1.96$, then the null hypothesis is rejected.

B Pearson Correlation Coefficients and Fisher Transformation

To find the Pearson Correlation between two regions, we take the time series for both and use the equation below to calculate their correlation to one another:

$$r = \frac{\sum_{i=1}^{n}(X_i - \bar{X})(Y_i - \bar{Y})}{\sqrt{\sum_{i=1}^{n}(X_i - \bar{X})^2 (Y_i - \bar{Y})^2}} \tag{C.5}$$

where $\bar{X}$ and $\bar{Y}$ are the means of the times series X and Y, respectively and n is the number of time points.

Once r was obtained for each pairing of regions for each participant, a Fisher Transformation was used to normalize the values for comparison. The Fisher Transformation formula's

for going to and from z are below:

$$z = arctanh(r) \tag{C.6a}$$

$$r = tanh(z) \tag{C.6b}$$

While all scores were in z form, they were compared using a t-test using the follow equation

$$t = \frac{\bar{X}_1 - \bar{X}_2}{s_\Delta} \tag{C.7}$$

where

$$s_\Delta = \sqrt{\frac{s_1^2}{n_1} + \frac{s_2^2}{n_2}} \tag{C.8}$$

After comparison, the average z value for each connection for each group was transformed back using the above transformation.

C Conditional Granger Causality (Dhamala et al. (2008), Wen et al. (2013))

Consider two time series X_t and Y_t represented by the bivariate autoregressive models:

$$\begin{aligned} X_t &= \sum_{j=1}^{\inf} a_{1j} X_{t-j} + \sum_{j=1}^{\inf} b_{1j} Y_{t-j} + \varepsilon_{1t} \\ Y_t &= \sum_{j=1}^{\inf} c_{1j} X_{t-j} + \sum_{j=1}^{\inf} d_{1j} Y_{t-j} + \eta_{1t} \end{aligned} \tag{C.9}$$

The pairwise Granger Causality from Y to X is defined as:

$$F_{y \to x} = ln \frac{\Sigma_X}{\Sigma_{xx}} \tag{C.10}$$

where Σ_X and Σ_{xx} are the error covariances in the two predictions. If $F_{y\to x} > 0$ then Y has a causal effect on X. However, if there were more than two time-series, then this calculation would be insufficient as it would find a causal effect for indirect paths to X. If we now consider that there are three time-series X_t, Y_t, and Z_t to determine if the influence of Y on X is direct then Z_t must be factored in to determine this. These three time-series would have the joint and trivariate autoregressive models:

$$\begin{aligned} X_t &= \sum_{j=1}^{\inf} a_{2j} X_{t-j} + \sum_{j=1}^{\inf} b_{2j} Z_{t-j} + \varepsilon_{2t} \\ Z_t &= \sum_{j=1}^{\inf} c_{2j} X_{t-j} + \sum_{i=1}^{\inf} d_{2j} Z_{g-j} + \zeta_{2t} \end{aligned} \tag{C.11}$$

and

$$\begin{aligned} X_t &= \sum_{j=1}^{\inf} a_{3j} X_{t-j} + \sum_{j=1}^{\inf} b_{3j} Y_{t-j} + \sum_{j=1}^{\inf} c_{3j} Z_{t-j} + \varepsilon_{3t} \\ Y_t &= \sum_{j=1}^{\inf} d_{3j} X_{t-j} + \sum_{i=1}^{\inf} e_{3j} Y_{t-j} + \sum_{i=1}^{\inf} g_{3j} Z_{g-j} + \eta_{3t} \\ Z_t &= \sum_{j=1}^{\inf} u_{3j} X_{t-j} + \sum_{i=1}^{\inf} w_{3j} Y_{t-j} + \sum_{i=1}^{\inf} v_{3j} Z_{g-j} + \zeta_{3t} \end{aligned} \tag{C.12}$$

The two joint pairing give the following covariance matrices:

$$\Sigma_{(X,Y)} = \begin{pmatrix} \Sigma_1 & \gamma_1 \\ \gamma_1 & \Gamma_1 \end{pmatrix} \Sigma_{(X,Z)} = \begin{pmatrix} \Sigma_2 & \gamma_2 \\ \gamma_2 & \Gamma_2 \end{pmatrix} \tag{C.13a}$$

And the trivariate model produces the covariance matrix:

$$\Sigma_{(X,Y,Z)} = \begin{pmatrix} \Sigma_{xx} & \Sigma_{xy} & \Sigma_{xz} \\ \Sigma_{yx} & \Sigma_{yy} & \Sigma_{yz} \\ \Sigma_{zx} & \Sigma_{zy} & \Sigma_{zz} \end{pmatrix} \tag{C.14}$$

Using these matrices similar to pairwise, we can calculate Y_t to X_t conditional on Z_t:

$$F_{Y\to X|Z} = ln\frac{\Sigma_2}{\Sigma_{xx}} \tag{C.15}$$

If $f_{Y\to X|Z} > 0$ then this indicates Y_t has a direct causal influence to X_t. If $f_{Y\to X|Z} = 0$ then the connection from Y_t to X_t is entirely indirect and mediated by Z_t

The frequency form of this can be calculated using the following equation:

$$I_{Y\to X|Z}(f) = ln\frac{\Omega_{xx}}{Q_{xx}(f)\Sigma_{xx}Q^*_{xx}(f)} \tag{C.16}$$

where

$$Q(f) = \begin{pmatrix} Q_{xx}(f) & Q_{xy}(f) & Q_{xz}(f) \\ Q_{yx}(f) & Q_{yy}(f) & Q_{yz}(f) \\ Q_{zx}(f) & Q_{zy}(f) & Q_{zz}(f) \end{pmatrix} = G(f)^{-1}\cdot H(f) \tag{C.17}$$

Here, $G(f)$ is the transfer function matrix for the joint autoregressive model for X_t and Z_t and $H(f)$ is the transfer function matrix for the trivariate autoregressive model for X_t, Y_t and Z_t